

Markus Heggås

# Dynamic Rating of Power Cables Based upon Transient Temperature Calculations

Master's thesis in Energy Use and Energy Planning

Supervisor: Erling Ildstad

June 2019



Markus Heggås

# Dynamic Rating of Power Cables Based upon Transient Temperature Calculations

Master's thesis in Energy Use and Energy Planning  
Supervisor: Erling Ildstad  
June 2019

Norwegian University of Science and Technology  
Faculty of Information Technology and Electrical Engineering  
Department of Electric Power Engineering





## Hovedoppgave Våren 2019

Kandidatens navn: Markus Heggås

Fag: Electric Power Engineering

Oppgavens tittel (norsk): **Estimering av kraftkablens dynamiske belastningsevne basert på transiente temperaturberegninger.**

Oppgavens tittel (engelsk): **Dynamic rating of power cables based upon transient temperature calculations**

Traditionally the current load capacity or ampacity of a cable system is limited by the maximum allowed conductor temperature, expected to occur during long-term steady state maximum current load. In practice, most power cables operate at service temperatures far below this maximum design temperature. Recent simulations and measurements have shown that, depending upon the operation and cable laying conditions, higher currents than the predefined maximum value can be applied for several hours or days before critical conductor temperatures occur. In principle, the heat capacity and cooling capacity of the cable surroundings, causing these long thermal time constants, represent an installed reserve in the power grid.

The main purpose of this Master thesis is to explore means of utilizing this, by for example periods of current “overload” based upon transient temperature calculations and measurements of critical temperatures and operation parameters.

The thesis is expected to constitute:

- A literature survey, forming the base for suggested methods for dynamic thermal design of power cable. Including theory for development of transient temperatures and expected excessive thermal degradation.
- A survey of what information a grid operator needs to utilize dynamic rating.

- A description of working principle and assumptions needed for transient temperature calculations, according to COMSOL Multiphysics and the IEC 60853 procedure. Comparison and evaluation of these procedures regarding accuracy and applicability.
- Presentations and comparisons of the main findings from calculated temperatures versus time and current load of selected cases.
- A discussion and conclusions regarding the validity, limitations and future application of the approach.

The details of the tasks are decided in cooperation with the supervisor.

Start: 8. January 2019  
Delivery: 11. June 2019  
Supervisor: Prof. Erling Ildstad  
(Erling.Ildstad@elkraft.ntnu.no)

---

# Preface

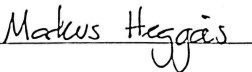
This thesis concludes my M.Sc. degree in Electric Power Engineering at the Norwegian University of Science and Technology (NTNU), carried out during the spring semester of 2019.

First of all, my sincere appreciation goes to my family, for being supportive and encouraging throughout my whole study period. A special thank you goes to my girlfriend, Margrét, for proofreading my thesis.

Further, I would like to direct my deepest gratitude to my supervisor, Professor Erling Ildstad, for the excellent support and guidance I have received during the whole thesis period. In addition, I would like to thank my fellow students at the Department of Electric Power Engineering for all the amusing lunch breaks throughout my five years as a student. My deepest gratitude also goes to the fantastic professors at NTNU for all the knowledge I have gained from your interesting lectures.

Trondheim, June 2019

Markus Heggås



---

# Abstract

Existing current rating methods are generally based on worst case assumptions of weather conditions (high ambient temperature) and steady-state loading (100% load factor). Due to large thermal masses, variations in ambient conditions and the fact that steady-state loading is seldom applied, it is often feasible to overload power system components to some extent for a certain amount of time. In this sense, the ampacity of power system components, such as power cables, can be considered dynamic.

In this thesis, a literature review is performed to give an overview of experience and applications of dynamic ratings systems. Further, an analytical thermal model is developed according to the IEC standards for rating of power cables. The aim for the thesis is to investigate for how long and to what extent a power cable can be overloaded in various case examples. Moreover, it is evaluated how information about sheath temperature, ambient conditions and load history can be utilized to estimate the conductor temperature. A part of the analysis is also to evaluate how increased temperatures due to overloading will inflict on the aging of the cable insulation.

To appraise the results from the analytical modeling approach, a numerical model in COMSOL Multiphysics is developed for comparison. The results show that transient temperature calculations from the analytical model compare well with the numerical model and are in good accordance with findings from other authors. The largest deviation between the two modeling approaches occurs approximately 30 minutes after a change in applied current.

The permitted overloading time period will vary with applied overload current, conductor temperature limit and load history. In the case of an initial load of rated current and a 90 °C conductor temperature limit, an overload current of 60% (a current 60% higher than rated current), can be applied for 30 hours.

The results show that an interpretation of sheath temperature measurements can be useful for estimating the conductor temperature. Such information may be obtained by measuring the time derivative of sheath temperature.

Moreover, a 10 °C step change in air temperature lasting for 100 hours will only increase the soil temperature at burial depth with 1 °C. This slow impact of air temperature at burial depth justifies that it is only necessary to consider seasonal variations of soil temperatures during transient overloading.

Lastly, it is shown that the additional aging caused by operating at elevated temperatures can be estimated. In the case of an overload current of 83% applied for 24 hours, the cable lifetime is reduced by approximately one month. This is only 0.2% of the total expected cable lifetime of 40 years.



---

# Sammendrag

Dagens metoder for beregning av strømbelastningsevne er generelt basert på konservative anslag for omgivelsestemperatur og kontinuerlig maks belastning. På grunn av termisk treghet, variasjoner i omgivelsesforhold, og det faktum at maks belastning sjelden er påtrykt, er det i perioder forsvarlig å overbelaste kraftkomponenter til en viss grad. I den forstand kan belastningsevnen til komponenter i kraftnettet, som for eksempel kraftkabler, betraktes som dynamisk.

I denne masteroppgaven er utført en litteraturstudie for å gi en oversikt over erfaringer og bruksområder for dynamisk belastningsevne. Det er utviklet en analytisk termisk modell i henhold til IEC-normer for beregning av belastningsevne for kraftkabler. Formålet med oppgaven er å undersøke hvor lenge og til hvilken grad en kraftkabel kan bli overbelastet i ulike scenarioer. Videre er det evaluert hvordan informasjon om kappetemperatur, omgivelsesforhold og lasthistorikk kan brukes for å anslå ledertemperaturen. En del av oppgaven er også å anslå den ytterligere aldringen økt temperatur, som følge av overbelastning, vil påføre kabelisolasjonen.

For å gjøre en vurdering av resultatene fra den analytiske modellen, er de sammenlignet med beregninger fra en numerisk modell utviklet i COMSOL Multiphysics. Resultatene fra de transiente temperaturberegningene for den analytiske modellen samsvarer godt med den numeriske modellen, og er i god overensstemmelse med lignende resultater fra litteraturen. Den største temperaturforskjellen mellom de to beregningsmetodene inntreffer omtrent 30 minutter etter en endring i påtrykt strøm.

Tillatt varighet av overbelastning vil variere med påtrykt overlaststrøm, restriksjoner på ledertemperatur og lasthistorikk. Med nominell strøm som startbetingelse og maksimal ledertemperatur på 90 °C, kan en overlaststrøm på 60% (en strøm 60% høyere enn nominell strøm), påtrykkes i 30 timer.

Resultatene viser at måledata for den tidsderiverte av kappetemperatur kan utnyttes til å estimere ledertemperaturen. Videre viser simuleringene at en 10 °C temperaturøkning i utetemperatur med varighet på 100 timer, bare vil føre til en temperaturøkning på 1 °C ved kabelens forleggingsdybde. Den langsomme innvirkningen utetemperatur har ved forleggingsdybden rettferdiggjør at det bare trengs å ta hensyn til sesongvariasjoner av jordsmonntemperatur ved kortvarige overbelastninger.

Resultatene viser også at den ytterligere aldringen som følge av økt temperatur kan beregnes. En overbelastningsstrøm på 83% med varighet av 24 timer vil redusere kabelens levetid med én måned. Dette tilsvarer en reduksjon på kun 0.2% av kabelens totale levetid på 40 år.

---

# Table of Contents

<b>Preface</b>	<b>i</b>
<b>Abstract</b>	<b>ii</b>
<b>Sammendrag</b>	<b>iii</b>
<b>Table of Contents</b>	<b>vii</b>
<b>List of Tables</b>	<b>ix</b>
<b>List of Figures</b>	<b>xiii</b>
<b>List of Symbols and Abbreviations</b>	<b>xv</b>
<b>1 Introduction</b>	<b>1</b>
1.1 Background and motivation . . . . .	1
1.2 Dynamic rating principle . . . . .	3
1.3 Scope and problem definition . . . . .	4
<b>2 Literature review of dynamic rating</b>	<b>5</b>
2.1 Temperature monitoring of cables and overhead lines . . . . .	6
2.2 Examples of dynamic rating for overhead lines . . . . .	7
2.3 Examples of dynamic rating for cables . . . . .	9
2.4 Grid operators' use of dynamic rating . . . . .	12
<b>3 Thermal modeling of power cables</b>	<b>15</b>
3.1 Conventional cable rating standards . . . . .	16
3.2 Establishing the cable thermal equivalent . . . . .	16
3.2.1 Thermal resistance of the cable parts and surrounding soil . . . . .	17
3.2.2 Heat capacitance of the cable parts . . . . .	19
3.2.3 Resulting thermal equivalent . . . . .	20
3.3 Transient cable conditions . . . . .	21

---

3.3.1	Temperature rise in the internal parts of the cable . . . . .	21
3.3.2	Cable environment impact on the temperature rise . . . . .	22
3.3.3	Resulting temperature rise . . . . .	23
3.3.4	Temperature dependent resistance of the conductor . . . . .	23
3.3.5	Transient temperature rise under variable loading (Superposition principle) . . . . .	24
<b>4</b>	<b>Thermal aging of cable insulation</b>	<b>25</b>
4.1	Thermal aging due to chemical degradation . . . . .	26
4.2	Thermal degradation over an overload period . . . . .	27
<b>5</b>	<b>Analytical and numerical thermal model of a single-core XLPE cable</b>	<b>29</b>
5.1	Analytical modeling based on the IEC standards . . . . .	31
5.1.1	Conductor temperature rise . . . . .	33
5.1.2	Sheath temperature rise . . . . .	35
5.1.3	Cable environment impact on the temperature rise . . . . .	37
5.1.4	Resulting calculation algorithm based on IEC standards . . . . .	38
5.1.5	Temperature response of multi-step loads . . . . .	39
5.2	Numerical modeling in COMSOL . . . . .	40
5.2.1	Model geometry . . . . .	40
5.2.2	Material properties of the cable parts and its surroundings . . . . .	42
5.2.3	Physics interface and solver modules . . . . .	43
5.2.4	Boundary conditions . . . . .	44
5.2.5	Meshing . . . . .	46
<b>6</b>	<b>Overloading case examples</b>	<b>47</b>
6.1	Overloading capacity with various combinations of overloading current and initial load . . . . .	47
6.2	Permitted overloading for 6 hours and 24 hours . . . . .	48
6.3	Additional aging during overload conditions . . . . .	48
<b>7</b>	<b>Results and discussion</b>	<b>51</b>
7.1	Comparison of the analytical and numerical modeling approach . . . . .	52
7.1.1	Step response of a step current from a no-load condition . . . . .	52
7.1.2	Step response of a full-load-to-no-load step current from a no-load condition . . . . .	53
7.1.3	Discussion on the comparison of the analytical and numerical modeling approach . . . . .	55
7.2	Transient temperatures under variable loading . . . . .	57
7.3	Overload conditions with varying load history prior to overloading . . . . .	58
7.3.1	Time to reach maximum permitted conductor temperature . . . . .	59
7.3.2	Conductor temperature vs. measurable sheath temperature . . . . .	61
7.3.3	Effect of increasing the maximum conductor temperature limit . . . . .	63
7.4	Overload case example - 6 hours and 24 hours overloading . . . . .	64
7.4.1	Permitted overloading profiles based on temperature limits . . . . .	64
7.4.2	Thermal aging due to overloading profiles . . . . .	66

---

---

7.5	Temperature variations in the soil . . . . .	67
7.5.1	Air ambient temperature influence on soil temperature . . . . .	67
7.5.2	Impact of seasonal variations of the soil . . . . .	69
<b>8</b>	<b>Conclusions</b>	<b>71</b>
<b>9</b>	<b>Further work</b>	<b>73</b>
	<b>Bibliography</b>	<b>73</b>
	<b>Appendix A - Calculation of conductor and sheath temperature</b>	<b>83</b>
	<b>Appendix B - Nomograms for exponential integral</b>	<b>87</b>
	<b>Appendix C - Overloading example</b>	<b>88</b>
	<b>Appendix D - MATLAB source code</b>	<b>89</b>

---

# List of Tables

2.1	Parameters measured by the most common measuring devices for overhead lines. . . . .	7
5.1	Data for a single core 10 kV cable. . . . .	30
5.2	Material properties of the cable parts and the surrounding soil used in the analytical modeling approach. . . . .	31
5.3	Lumped parameters calculated based on IEC 60853. . . . .	32
5.4	Calculated values of the thermal resistances and heat capacitances in figure 5.3. . . . .	32
5.5	Calculated parameters from equation 5.4 - 5.9 used in the conductor temperature rise calculation. . . . .	34
5.6	Data for different parameters used in calculation of the temperature dependent conductor resistance. . . . .	34
5.7	Values of coefficients $T_{21}$ and $T_{21}$ in calculations of sheath temperature rise. . . . .	36
5.8	Thermal conductivity, heat capacity and density for the cable materials and surround soil used in COMSOL simulations. . . . .	43
6.1	Aging rates for various operating temperatures for XLPE insulation. . . . .	48
6.2	Total lifetime consumption (aging) of the cable lifetime due to the temperature profile in figure 6.2. . . . .	50
7.1	Time to reach maximum permitted conductor temperature ( $\theta_c^{max}$ ) and sheath temperature at $\theta_c^{max}$ for different combinations of initial loading and overloading. . . . .	59
7.2	Time to reach 100 °C and 110 °C conductor temperature for different combinations of initial load and overloading. . . . .	63
7.3	Total aging due to overload profiles in figure 7.13. . . . .	66

---



# List of Figures

2.1	Utilities answer on the question "Reason for using a temperature measuring equipment". . . . .	6
2.2	Rating capacity of an overhead line in different rating schemes. . . . .	8
2.3	Measured and calculated cable surface and conductor temperature with a multi-step load over a period of eight days. . . . .	10
2.4	Predicted conductor temperature under different overloading conditions. . . . .	10
2.5	Comparison conductor temperature and sheath temperature calculated by a FEM method (COMSOL) and a network model based on IEC standards. . . . .	11
2.6	One hour emergency rating vs. starting conductor temperature. . . . .	12
3.1	Cross section a the single-core power cable with a conductor, insulation layer, metallic screen and protective sheath. . . . .	20
3.2	Transient thermal equivalent of the power cable in figure 3.1. . . . .	20
3.3	Illustration of the principle of superposition to calculate the resulting temperature rise due to two step current (one step up and one step down). . . . .	24
4.1	Arrhenius plot used for estimating cable lifetime at service temperatures. . . . .	27
5.1	Cross section of the single core cable used in the modeling. . . . .	30
5.2	Transient thermal equivalent of cable in figure 5.1 directly buried. . . . .	31
5.3	Two-loop thermal equivalent for temperature calculations. . . . .	32
5.4	Temperature dependent resistance for a 300 mm <sup>2</sup> copper conductor. . . . .	35
5.5	Flow chart of the developed algorithm for conductor and sheath temperature rise calculations based on IEC standards for cable ratings. . . . .	38
5.6	Total transient temperature response of multiple load steps calculated by the Superposition principle. . . . .	39
5.7	Total domain and burial depth of the cable of in the COMSOL model. . . . .	40
5.8	Steady-state conductor temperature as a function of domain size. . . . .	41
5.9	Conductor temperature as a function of time for different domain sizes. . . . .	41
5.10	Cross section of the 10 kV single core cable in COMSOL. . . . .	42

---

5.11 Isothermal boundary condition (constant temperature of 15 °C at the soil surface). . . . .	44
5.12 Thermal insulation boundary condition applied to the soil part of the domain. . . . .	45
5.13 Illustration of the mesh for the cable and its surroundings. The mesh density is high near the cable . . . . .	46
6.1 Aging rate for an XLPE insulated cable . . . . .	49
6.2 Conductor temperature in a simplified case. . . . .	50
7.1 Transient temperature response for a full-load step current (700 A) applied for 1000 hours, to compare the analytical algorithm with the COMSOL model. Prior to the current step, the cable was unenergized, <i>i.e.</i> , both the conductor and sheath were at an ambient temperature of 15 °C. . . . .	52
7.2 Deviation between the analytical algorithm and the COMSOL model for conductor and sheath temperature calculations. A full-load step current (700 A) is applied for 1000 hours. . . . .	53
7.3 Transient temperature response to compare the analytical algorithm with the COMSOL model. A full-load step current (rated current) is applied for 50 hours, followed by a no-load condition for another 50 hours. . . . .	54
7.4 Deviation between the analytical algorithm and the COMSOL model for conductor and sheath temperature calculations. A full-load step current (rated current) is applied for 50 hours, followed by a no-load condition for another 50 hours. . . . .	54
7.5 Conductor temperature response with three different values of soil diffusivity. . . . .	55
7.6 Conductor temperature rise above ambient for the first hour after applying a step load of rated current. . . . .	56
7.7 Transient temperature calculations with various thermal resistivity of soil. . . . .	57
7.8 Conductor and sheath temperatures when applied a cyclic load current. . . . .	58
7.9 Transient conductor and sheath temperature the first half hour after applied an overload step current. Prior to the overload current, the average load is assumed to be 75% of rated current. . . . .	61
7.10 Time derivative of conductor and sheath temperature for the first hour of overloading at 60%, showing the rate of which the temperatures are changing. . . . .	62
7.11 Permitted overload current for a period of 6 hours and 24 hours with maximum conductor temperature limits of 90 °C, 100 °C and 110 °C. . . . .	64
7.12 Conductor temperature after 6 hours of overloading at 78, 87 and 96% above rated current as a function of initial load. . . . .	65
7.13 Overloading profiles of 6 hours and 24 hours for maximum temperature of 90 °C, 100 °C and 110 °C. Initial load prior to overloading is 75% of rated current. . . . .	66
7.14 Soil surface temperature and temperature development at burial depth for a step increase in air ambient temperature of 10 °C (from 15 °C to 25 °C) for 5000 hours. . . . .	68

---

---

7.15	Temperature development at burial depth for a step increase in air ambient temperature for 100 hours. . . . .	68
7.16	Impact of seasonal variations in summer and winter temperature at burial depth. Winter temperature is assumed to be 0 °C, while summer temperature is set to 15 °C. . . . .	69
C.1	Conductor temperature and time to reach maximum allowed conductor temperature for different overload scenarios. Average load prior to overloading was assumed to be 75% of rated current until steady-state conditions were obtained. . . . .	88

---

# List of Symbols and Abbreviations

Symbol	Unit	Description
$A$	[mm <sup>2</sup> ]	Area
$A_c$	[mm <sup>2</sup> ]	Conductor area
$L$	[mm]	Cable burial depth
$l$	[mm]	Cable length
$t_i$	[mm]	Thickness of layer $i$
$t_s$	[mm]	Sheath thickness
$t_{ins}$	[mm]	Insulation thickness
$D_i$	[mm]	Diameter beneath layer $i$
$D_{ex}$	[mm]	External diameter of a layer
$D_{in}$	[mm]	Inner diameter of a layer
$D_{ins}$	[mm]	Insulation diameter
$D_c$	[mm]	Conductor diameter
$D_s$	[mm]	Internal sheath diameter
$D_e$	[mm]	Cable diameter
$\rho_i$	[K·m/W]	Thermal resistivity of material $i$
$\rho_{soil}$	[K·m/W]	Thermal resistivity of soil
$\rho_{ins}$	[K·m/W]	Thermal resistivity of insulation
$\rho_s$	[K·m/W]	Thermal resistivity of sheath
$T_i$	[K·m/W]	Thermal resistance of layer $i$
$T_1$	[K·m/W]	Thermal resistance of insulation
$T_2$	[K·m/W]	Thermal resistance of metallic screen
$T_3$	[K·m/W]	Thermal resistance of sheath
$T_4$	[K·m/W]	Thermal resistance of soil
$T'_4$	[K·m/W]	Thermal resistance of air between cable surface and duct
$T''_4$	[K·m/W]	Thermal resistance of duct
$T'''_4$	[K·m/W]	Thermal resistance of duct surroundings

---

$T_A$	[K·m/W]	Two-loop equivalent thermal resistance of first loop
$T_B$	[K·m/W]	Two-loop equivalent thermal resistance of second loop
$Q$	[J/K·m]	Heat capacitance
$Q_{ins}$	[J/K·m]	Heat capacitance of insulation
$Q_c$	[J/K·m]	Heat capacitance of conductor
$Q_{scr}$	[J/K·m]	Heat capacitance of metallic screen
$Q_s$	[J/K·m]	Heat capacitance of sheath
$Q_A$	[J/K·m]	Two-loop equivalent thermal capacitance of first loop
$Q_B$	[J/K·m]	Two-loop equivalent thermal capacitance of second loop
$C_v$	[J/K·m <sup>3</sup> ]	Volumetric heat capacity
$C_p$	[J/kg·K]	Heat capacity at constant pressure
$C_{p,soil}$	[J/kg·K]	Heat capacity of soil at constant pressure
$\delta$	[m <sup>2</sup> /s]	Diffusivity of soil
$d$	[kg/m <sup>3</sup> ]	Density
$d_{soil}$	[kg/m <sup>3</sup> ]	Density of soil
$\lambda$	[W/K·m]	Thermal conductivity
$\lambda_{soil}$	[W/K·m]	Thermal conductivity of soil
$W_c$	[W/m]	Conductor loss per meter
$W_{conv,s}$	[W/m]	Convection heat transfer between the cable and surroundings
$W_{cond}$	[W/m]	Conduction heat transfer in the cable surroundings
$W_{rad,s-w}$	[W/m]	Radiation heat transfer between the duct and cable surface
$q$	[W/m <sup>2</sup> ]	Heat flux
$q_{cond}$	[W/m <sup>2</sup> ]	Heat flux by conduction
$q_{rad}$	[W/m <sup>2</sup> ]	Heat flux by radiation
$\rho_{c,20}$	[Ω·m]	Electrical resistivity of conductor at 20 °C
$Z_{tot}$	[Ω]	Total impedance two-loop equivalent
$Z_b$	[Ω]	Total impedance "downstream" of second node
$R_\theta$	[Ω]	Temperature dependent conductor resistance
$R_{20}$	[Ω]	Conductor resistance at 20 °C
$I$	[A]	Current
$\theta$	[°C]	Temperature
$\theta_0$	[°C]	Reference temperature
$\theta_s$	[°C]	Sheath temperature
$\theta_w$	[°C]	Duct inner surface temperature
$\theta_m$	[°C]	Temperature rise at node $m$
$\theta_e$	[°C]	Temperature rise due to soil

---

---

$P_j, P_k$	$[s^{-1}]$	Time constants from poles of the transfer function
$a$	$[s^{-1}]$	Time constant
$b$	$[s^{-1}]$	Time constant
$M_0$	$[s]$	Variable used to simplify equations
$N_0$	$[s^2]$	Variable used to simplify equations
$k_B$	$[eV/K]$	Boltzmann's constant
$w$	$[eV]$	Activation energy
$R_a$	$[% h^{-1}]$	Aging rate as a function of temperature
$L_f$	$[%]$	Loss of life
$L(\theta)$	$[h]$	Lifetime as a function of temperature
$L_0$	$[h]$	Lifetime at reference temperature
$t$	$[h]$	Time
$t_D$	$[h]$	Time duration
$r$		Rate of chemical reaction
$r'$		Constant for Arrhenius' equation
$\gamma$		Attainment factor
$N$		Normal vector of the boundary surface
$H(s)$		Transfer function of thermal equivalent
$Y(s)$		Output of transfer function
$X(s)$		Input of transfer function
$Z_{km}$		Zeros of transfer function
$T_{m,j}$		Coefficient from the thermal equivalent
$x_{(n-m)m}$		Coefficient of the numerator of transfer function
$y_n$		First coefficient of the denominator of transfer function
$p$		Van Wormer coefficient for insulation
$p'$		Van Wormer coefficient for sheath
$-Ei(x)$		Exponential integral
$K$		Interval
$n$		Number of loops
$i$		Index
$m$		Node index
$j$		Index from 1 to $n$
$k$		Index from 1 to $n$ , $k \neq j$
$\frac{\partial}{\partial x}$		Temperature gradient in $x$ direction
$\frac{\partial}{\partial y}$		Temperature gradient in $y$ direction
XLPE		Cross-linked polyethylene
PE		Polyethylene
FEM		Finite element method
IEC		International Electrotechnical Commission
DTS		Distributed temperature sensing
SCADA		Supervisory Control and Data Acquisition
CMARS		Cable Monitoring and Rating System

---

---

EPRI  
ICT  
DC  
AC

Electric Power Research Institute  
Information and communications technology  
Direct current  
Alternating current



# Chapter 1

## Introduction

This chapter first provides an introduction where the underlying background and motivation for the thesis is given. Further, the chapter gives a description of the principle of dynamic rating. Finally, the problem definition and scope of the thesis is described.

### 1.1 Background and motivation

Due to higher energy demand, the global electricity generation has grown rapidly the past decades [1]. According to Liu [2], the annual growth rate of generated electricity has been 3.2% since 1990. It is foreseen that future electricity supply will have a higher share of renewable electricity production, where forecasting electricity generation can be difficult [3]. These changes require higher capacity, both long-term and periodically, in the power transmission system. Costly structural refurbishments are hence needed in the power system to meet these requirements [4].

To avoid excessive thermal aging due to operating temperatures exceeding their limits, correct ampacity rating of power system components, such as power cables, is important. The ampacity is defined as the maximum current that can be carried without violating these limits. Correct ampacity of a power cable depends on choosing proper values for the thermal properties of the surrounding soil and accurately describing the ambient conditions.

The power failure in Auckland in 1998 showed the difficulty of choosing appropriate values of the thermal resistivity to ensure reliable operation of power cables. Unusual hot and dry weather in conjunction with high load increased the thermal resistivity of the bedding, causing the cable temperature to rise higher than the permitted limits. Which in

turn caused deterioration of the insulation material that led to cable failure. It took five weeks to restore the power supply, causing big economic losses for the local businesses [5].

To avoid premature aging of the insulation material, the operating temperature limit of cross-linked polyethylene (XLPE) cables is usually restricted to 90 °C [6]. Extruded cables that are overheated for a period of time may suffer from deformation (thermal expansion) of the insulating material. Deterioration of the insulation decreases the electric strength, which in turn can initiate a breakdown [7].

The aging and thus lifetime of cables is however influenced by several other mechanisms, such as electrical stress, mechanical stress, and the environment the insulation is subjected to. For electrical power equipment, it is reasonable to consider a lifetime of 30 - 40 years. Because of the long expected lifetime, it is evident that accelerated life tests are needed to determine how high stresses can be applied during service. In such tests, stresses are increased beyond what is assumed to be operating conditions, and the lifetime at operating condition is found by extrapolation [8, 9].

Ampacity of power components is often set with static thermal limits based on conservative heat transfer assumptions, worst case scenarios of ambient conditions and maximum load factor [10]. Up until recently, these static ratings have been sufficient since electricity production and consumption have been predictable. However, the increased usage of intermittent energy sources, such as wind and solar energy, makes it difficult to predict the needed power transmission capacity. Thus, conventional static rating methods, such as the International Electrotechnical Commission (IEC) 60287 standard, may no longer be adequate.

Weather conditions vary significantly within time and ambient temperature of power system components such as cables, overhead lines and transformers is usually lower than the conservative assumption in the IEC standard. Due to large thermal masses, it is often feasible to overload a power system component to some extent and for a certain amount of time without violating the thermal limits. Based on the limitations of the conventional rating methods, the ampacity of power system components is often underestimated.

By gaining better understanding of the dynamics in heating of power system components, asset utilization can be optimized. In this thesis, it is developed an analytical model according to the IEC standards for rating of power cables, to calculate transient temperatures of a cable. The aim was to investigate for how long and to what extent a power cable can be overloaded in various case examples. To appraise the results from the analytical modeling approach, a numerical model in COMSOL Multiphysics is developed for comparison.

## 1.2 Dynamic rating principle

The large thermal masses of power system components and varying ambient conditions make the ampacity rating of power system components variable. These variable ratings are referred to in the literature as "dynamic" or "real-time". In this thesis, the term "dynamic rating" is used.

A dynamic rating approach utilizes real-time ambient temperature and loading information [11]. For underground cables, the surface temperature of the cable could also be measured to better estimate the operating conductor temperature. Numerous utilities have installed optical fibers for distributed temperature sensing (DTS) systems that allow real-time monitoring of the temperature profile along the whole cable length [12]. Such systems can identify hot spots along a cable route to locate ampacity limiting sections of the power system.

Most grid operators don't have sufficient information to know the operating conductor temperature. Therefore, cable systems are often applied a lower current than the maximum permitted load, to ensure temperature limits are not violated. This means that there is an extra grid reserve present, that may be utilized by having more accurate temperature monitoring.

In conjunction with a dynamic thermal model of the ampacity limiting section, real-time determination of the operating thermal condition can help the system operator to make decisions regarding overloading of the power system. For situations where the actual capacity of the power system is greater than the conservative assumptions, dynamic rating can help increase the grid capacity [13].

The increased grid capacity a dynamic rating approach provides can have direct economic benefits for the utility by decreasing or delaying the need of costly refurbishments. A more efficient power transmission would also benefit the society and environment with lower tariff levels, cheaper connection to renewable energy production and less emissions associated with component production [4]. Furthermore, cost efficient solutions and higher reliability are required by the quality regulations in many countries (*e.g.* Norway) [14]. Therefore, smart structural investments, such as dynamic rating, are needed to increase the overall efficiency of the future power grid.

### 1.3 Scope and problem definition

In this thesis, a literature review is performed to give an overview of experience and applications for dynamic ratings systems. Further, an analytical algorithm to calculate transient sheath and conductor temperatures is compiled based on thermal modeling of cables from international standards for rating of electric power cables. To appraise the results from the analytical modeling, a numerical model is developed in COMSOL Multiphysics for comparison. From the developed transient thermal model, the main target of the thesis is to illuminate these research questions:

- How well do transient temperature calculations from an analytical modeling approach compare with a numerical model made in COMSOL?
- For how long and to what extent may the cable be overloaded without violating temperature limits of the conductor?
- How will the cable lifetime be affected by additional aging of the insulation material due to excessive heating caused by overloading?
- How can information about sheath temperature, loading history and ambient temperature be utilized to estimate transient conductor temperature for dynamic rating of a cable?

All simulations in the project will be performed on a directly buried 10kV single core XLPE cable based on Model Cable No.1 in Appendix A of Anders [15]. The cable is assumed to carry direct current (DC) current, thus screen loss and dielectric loss are not included. Moreover, it is assumed a cable circuit only consisting of one cable. Therefore, mutual heating of adjacent cables is not taken into account.

# Chapter 2

## Literature review of dynamic rating

In order to give an overview of experience and applications of dynamic rating systems, a comprehensive literature review was performed. The following chapter gives an introduction to how dynamic rating is applied to power systems and how case studies evaluate such a rating approach. The literature review summarizes the knowledge, development interests and research on use of dynamic rating in power systems.

Due to the high investment costs of cables, overhead lines and transformers, these components are of great interest in the literature on dynamic ratings. However, the dynamic rating approach is also applicable for other power equipment limited by thermal restrictions, such as switchgear [16]. To limit the research in this thesis, the literature review has mainly been on dynamic rating for cables and overhead lines, excluding dynamic rating for transformers. Nevertheless, transformers are among the most important elements in the power system and represent a significant portion of capital investment costs. A better rating solution for transformers, as well as for cables and overhead lines, may therefore defer the installing of new transmission circuits and thus be economically beneficial for grid operators. Some case studies on dynamic rating for transformers can be found in [17–20].

In the literature, the focus on dynamic rating has mainly been on overhead lines, whereas less attention has been paid to underground cables. Dynamic rating for overhead lines based on weather data is a state-of-the-art concept and commercial applications are available [21]. For underground cables however, dynamic rating based on weather data is more complicated due to thermal properties of the soil [4]. Therefore, most of the research on dynamic rating for cables is case studies and development concepts. However, some grid operators have implemented dynamic rating systems based on temperature measurements on a few cable systems [22].

## 2.1 Temperature monitoring of cables and overhead lines

An important part of the dynamic rating approach is to have accurate methods to monitor the operating temperature. This section therefore presents the most used temperature monitoring methods for overhead lines and power cables.

In the earliest studies of dynamic rating, sections of the cable where hot spots might be formed were equipped with thermocouples to measure the temperature [23–25]. This is however a time-consuming and difficult way of identifying hot spots along a cable route for complicated installations. By using optical fibers for temperature monitoring, hot spots and ampacity limiting sections where dynamic thermal rating should be applied can easily be detected [26]. A study from 1987 [27] showed that fiber optic cables for transferring data, such as temperature measurements, could be placed alongside power cables. The study also concluded that the additional costs of implementing an optical fiber while the power cable is being installed was negligible.

The usage of optical fibers for distributed temperature sensing (DTS) of power systems has increased in the past decades. In a report by Cigré [22], a survey of different grid operators showed that 96% of all temperature measuring equipment on power cables was DTS monitoring systems. The reasons for implementing such equipment varies widely, but the study showed that security, congestion, maintenance and dynamic rating are the main applications for DTS. However, the survey answers also concluded that in over 50% of the cases where DTS systems are installed, the grid operators answered "BLANK" on the question "Reason for using a temperature measuring equipment". This indicates that grid operators often install temperature monitoring systems without having a plan for utilizing the temperature data. Figure 2.1 shows how the utilities answered the question "Reason for using a temperature measuring equipment".

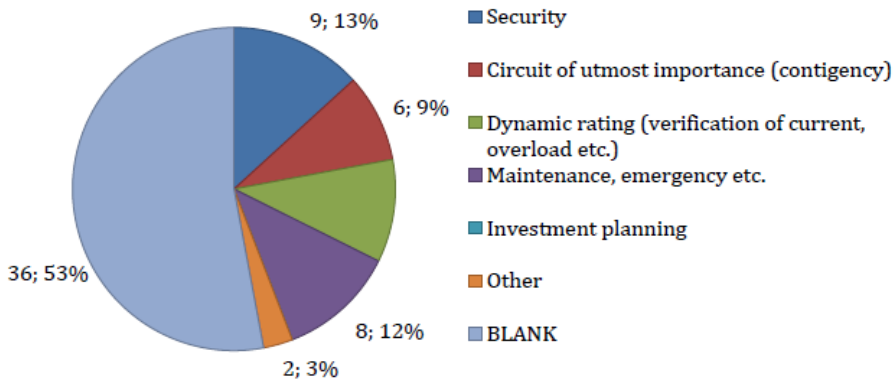


**Figure 2.1:** Utilities’ answer on the question "Reason for using a temperature measuring equipment" [22].

For insulated cables, the conductor temperature cannot directly be measured and must be calculated based on sheath temperature measurements. For overhead lines however, the conductor is laying in air and direct conductor measurements are accessible. Several commercial systems are available for line conductor temperature monitoring. Fernandez et al. [21] did a review of the most common conductor temperature applications for overhead lines. Most commercial measuring devices for overhead lines are connected directly to the conductor to measure the temperature or measure the tension or sag to calculate the conductor temperature. However, DTS systems based on embedded fiber optic cables are also available for overhead line conductors [28, 29]. The most common measuring devices and what they measure are listed in table 2.1 below. For more information on the different measuring devices and how they work, please refer to [21].

**Table 2.1:** Parameters measured by the most common measuring devices for overhead lines [21].

	<b>Conductor temperature</b>	<b>Current intensity</b>	<b>Tilt angle</b>	<b>Sag</b>
<b>Power Donut</b>	X	X	X	
<b>SMT</b>	X	X		
<b>OTLM</b>	X	X		
<b>TLM</b>	X		X	X
<b>FMC-T6</b>	X	X		
<b>EMO</b>	X			
<b>Ritherm</b>	X			

## 2.2 Examples of dynamic rating for overhead lines

Bare overhead line conductors are strongly affected by ambient conditions such as wind, temperature and solar irradiance. Dynamic ratings based on real-time monitoring of both weather and loading conditions have therefore captured attention of several researchers trying to unlock network capacities.

Davis [30] developed the first dynamic rating system for overhead lines using meteorological data, real-time conductor temperature and loading. The proposed method was in contrast to the conventional rating methods based on conservative weather (high ambient temperature and low wind speed) and loading assumptions. A system for dynamic rating for overhead lines had initially been conceived in the 1960s, but due to lack of Supervisory Control and Data Acquisition (SCADA) systems and conductor temperature sensing devices, it was not technologically feasible.

Paper [31] investigated dynamic rating for multi-span lines. It was shown that the dynamic rating of such lines is always less or equal to the rating of the individual spans. Since convective cooling varies along the line from span to span depending on the conductor orientation relative to the wind direction, it might be difficult to accurately rate long lines. It is therefore essential to have multiple monitoring points along a transmission line. Callahan and Douglass [32] showed that even for relatively short lines,

significant differences in thermal rating between the monitored spans were found.

Based on a monitoring device measuring line voltage, current and conductor temperature, the authors of [33] did an analysis of dynamic rating for overhead lines based on a Conductor Temperature Model, as opposed to the former Weather Model. The rating method was based on a well established dynamic thermal model of the conductor and its environment. The analysis confirmed that a dynamic rating system will provide increased line capacity and reduce the risk of overheating.

Safdarian et al. [11] investigated the grid reliability benefits dynamic rating has on distribution systems. It was found that the released capacity was greatest for overhead lines since they are much more affected by the weather conditions. Therefore, overhead lines may be rated in a more dynamic way than power components where ambient conditions are more stable (*e.g.* underground cables). The results showed that dynamic line rating solved almost all the generation curtailments due to distributed generation. It was also shown that a noteworthy portion of the benefits obtained by hourly ratings could be obtained by less dynamic, *e.g.* monthly and seasonal, ratings. The various rating capacities for the different dynamic thermal rating (DTR) versus the static thermal rating (STR) are shown in figure 2.2

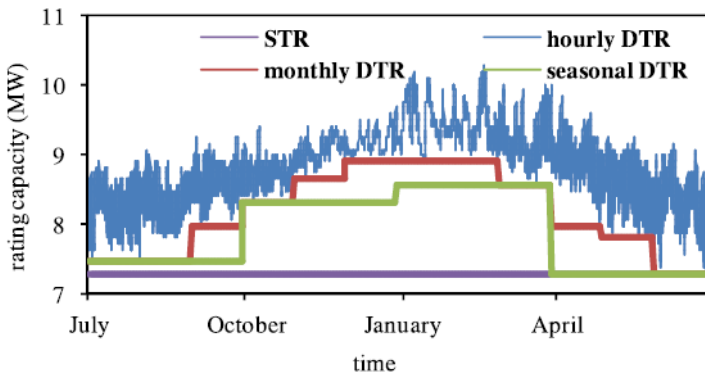


**Figure 2.2:** Rating capacity of an overhead line in different rating schemes [11].

Dynamic line rating for wind power integration has been of interest to researchers, since high production correlates positively with high wind speed and thus better cooling of lines, which in turn increases line capacity [4]. Many studies have therefore investigated how dynamic line ratings would impact wind power integration [21, 34–38]



## 2.3 Examples of dynamic rating for cables

Due to the high thermal mass of underground power cables, they may be overloaded to a certain extent without violating temperature limits of the insulation. This long thermal time constant represents a grid reserve that researchers have tried to utilize in a more optimal way.

In the late 1970s, Patton et al. [39] developed the Cable Monitoring and Rating System (CMARS) to estimate conductor temperature and thus rating of power cables. The dynamic model utilized measured conductor current and earth ambient temperature measurements to monitor cross-sectional temperature profiles. Based on these dynamic temperature profiles, continuous updates of the cable ratings were obtained. The CMARS approach therefore differed from earlier dynamic models, because it automatically calculated cable temperatures in real-time. Based on the principles established in the CMARS project, other dynamic rating systems have been developed [24, 25].

Paper [23] developed a method to compute conductor transient temperature based on the conductor current and cable sheath measurements. This system could be used to monitor actual conductor temperature or predict the conductor temperature based on load profiles. Since the cable sheath temperatures are measured continuously, any changes in the thermal conditions around the cable are monitored. This eliminates the need to evaluate thermal conditions which are external to the cable sheath. The accuracy of the developed calculation method was confirmed by a cable test installation where the conductor temperature was directly measured to compare with the calculated values.

Huang et al. [40] did the first attempt to incorporate forecasting data from a weather station for cable rating estimation. The dynamic cable rating system based on forecasting temperature resulted in better results than the traditional dynamic rating approaches based on constant temperature. Using meteorological data for soil temperature prediction has however been presented earlier in [41]. This reduces the associated error in rating calculations based on assumed ambient temperatures.

Reference [12] presented a general approach for real-time ratings of underground cables based on DTS measurements. For the identified hot spots on the cable, temperature measurements, installation information and load data were used to assess the cable ratings under normal and overload conditions. A combination of finite element method (FEM) and gradient-based optimization was used to accurately estimate soil thermal parameters. The method was validated by a laboratory set up and applied to a cable route. Figure 2.3 shows the measured and computed cable surface temperature and conductor temperature when a multi-step load is applied for a period of eight days. The results show that the computed temperatures correspond well with measured values.

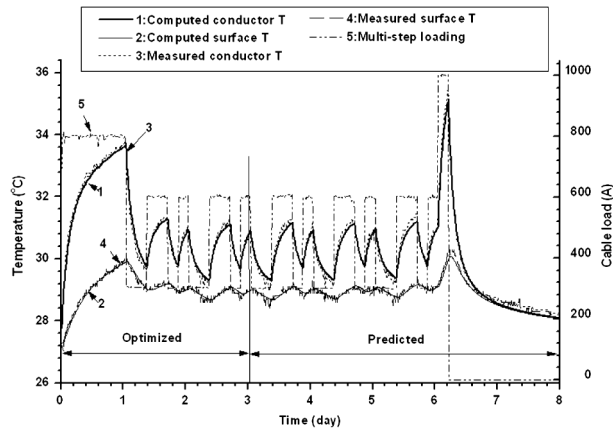


**Figure 2.3:** Measured and calculated cable surface and conductor temperature with a multi-step load over a period of eight days [12].

Li and Tan [12] also did an evaluation on the overload capacity of the ampacity limiting section of the cable. After the cable had been at variable loading for a period of time, it was subjected to overloads of 120%, 150% and 180% versus the nominal loading current of 1255 A. The predicted conductor temperature against time is shown in figure 2.4. A current 120% higher than rated current can be applied for as long as 45 hours without violating the 90 °C temperature limit.

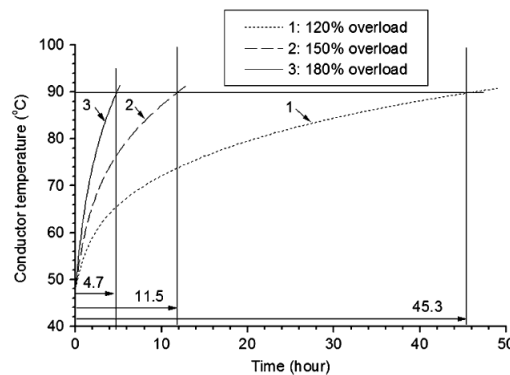


**Figure 2.4:** Predicted conductor temperature under different overloading conditions [12].

Anders et al. [42] purposed a more advanced dynamic rating technique for various constructions, installations and cable types. The computer program computes not only steady-state ratings and emergency ratings but also provides time required to attain a specified temperature. In addition, the paper included a model for heat transfer in cables laying in tunnel (air). Because of the low heat transfer rate by natural convection in cable sections laying in tunnels, this is often an ampacity limiting section of an underground

cable route. Therefore, dynamic rating systems should be applied in these sections. Other researches [43–48] have also investigated the thermal ratings for cables laying in air tunnels by modeling convection and radiation.

Based on DTS measurements and moisture content dependent thermal resistivity and specific heat of the cable surroundings, paper [49] developed an algorithm to estimated transient temperature evolution of power cables. The paper thereby presented an idea describing how cable operators at any given time can evaluate how much the cables can be loaded and for how long. The algorithm was verified by application to a cable system laboratory set up.

An improved dynamic rating system for transmission cable circuits was developed by Huang et al. [50]. This was achieved by a more accurate thermal model than the traditional IEC standard and prediction system for loading and ambient temperature. The ratings calculated by the improved model demonstrated a close match to a full FEM solution.

One doctoral dissertation [51] and a master’s thesis [8] have been investigating the overload capacity and transient cable temperatures by numerical and analytical modeling of cables. The comparison of a FEM solution and a simplified thermal network based on IEC standards for both projects is recalled in figure 2.5. The results show that the simple IEC model corresponds very well with a more complex numerical model.

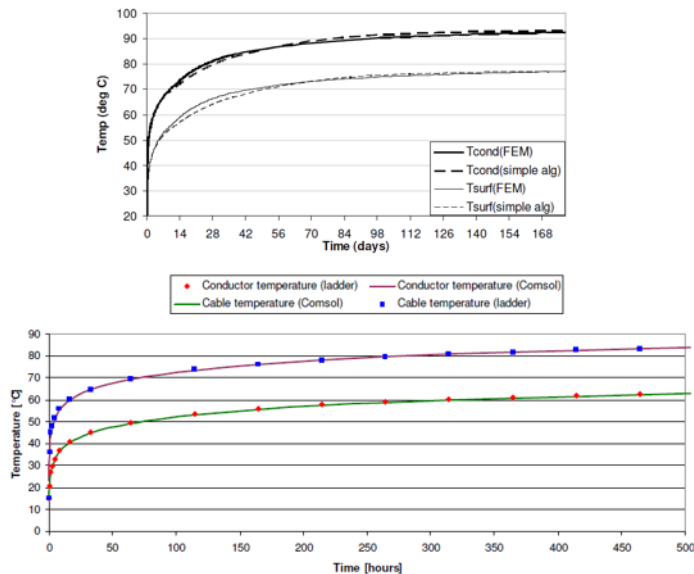


**Figure 2.5:** Comparison conductor temperature and sheath temperature calculated by a FEM method (COMSOL) and a network model based on IEC standards [8, 51]. The upper figure is found in [51] and the lowermost is found in [8].

## 2.4 Grid operators' use of dynamic rating

Dynamic rating systems let grid operators know the true thermal limits, which offer the benefit of utilizing existing power equipment to a greater extent. The dynamic rating systems also help the utility gain a better understanding of the system performance. Therefore, there is great interest of dynamic rating, both for underground cable and overhead lines, among the utilities [22, 52].

In the mid 1980s, the utility company Boston Edison installed the first commercial dynamic cable rating system, UPRATE<sup>tm</sup> [25], on a pair of 115 kV pipe cables connecting a downtown Boston substation to a generation plant. Later, because of the promising results, a second system was installed to another substation. The newly developed system permitted the utility to discard many of the standard conservative assumptions pertaining to the cable thermal environment and replace them with more accurate quantities.

Nelson et al. [25] investigated the effect starting temperature has on the emergency ratings of the cable circuit. This was in contrast to conventional emergency rating procedures, where starting temperature is assumed to be the maximum allowed temperature under worst-case assumptions. Figure 2.6 illustrates the effect starting temperature has on the one hour emergency rating using conductor temperature limits of 85 °C and 105 °C. The increased short-term transient ratings permitted the deferral of costly grid investments without sacrificing the reliability or integrity of the transmission supply.

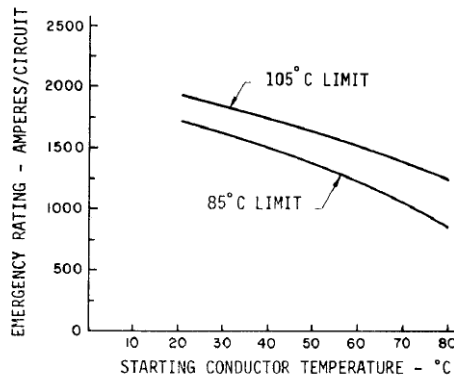


**Figure 2.6:** One hour emergency rating vs. starting conductor temperature [25].

A dynamic rating system developed by Electric Power Research Institute (EPRI) was deployed during a field test performed by an American utility. This system improved the rating of the existing power transmission circuits based on real-time weather and electrical current. The power capacity increased 5 - 15% with a software utilizing inexpensive and commercially available equipment, without the need for direct

measurement of equipment temperatures [16].

The submarine cable crossing between Norway and Denmark, Skagerrak 3, has since 1995 been equipped with a dynamic rating system based on DTS measurements [53]. Temperature data is transmitted to the control station where conductor and screen temperatures are calculated based on armor temperatures and actual conductor current. The rating system also calculates possible overload for the cable for the next 15, 30, 45 and 60 minutes. When conductor temperature reaches its limit, the system automatically lowers the power to the maximum nominal value. This is also done if the temperature difference between the conductor and the screen reaches a certain limit. A warning is given five minutes prior to the power reduction.

The interconnection between Norway and the Netherlands (NorNed) is also equipped by a dynamic rating system that calculates real-time conductor temperatures based on DTS measurements [54]. Optical fibers are placed outside the lead screen the first 5 kilometers or so from each land connection. The system has alarms connected to the operation center in case the temperatures get too high or rise too fast within a short time period. Currently, the system just monitors conductor temperatures to detect hot spots at an early stage to increase the reliability. Calculations of permissible overload for different time intervals are also available but not utilized.

Currently, there is no information and communications technology (ICT) structure available to utilize the dynamic rating calculations for overloading on the NorNed interconnection. Ground properties are changing with time, but the system has not been updated since commissioning, which makes the dynamic rating system data unreliable. Moreover, trained personnel or suppliers support is required to maintain and evaluate the data. For the cable interconnection operator, Statnett, information and data to the operation center should go through their SCADA platform. For security reasons, third party software from suppliers is not wanted [55]<sup>1</sup>.

The Belgium transmission system operator, Elia, also has experience with dynamic rating systems in combination with temperature sensing techniques. Optical fibers were integrated in the late 1990s for temperature monitoring, hot spot localization and verification of ampacity calculations. Due to the low loading, there was no direct need for dynamic rating to increase the transfer capacity. Now however, the load situation has changed because of decentralized and renewable energy production and several cables are already highly loaded. Therefore, the need to overload these cables beyond their static ratings is real. The real-time rating system is based on the IEC 60853 standard for cyclic rating [56].

---

<sup>1</sup>Personal communication with the Norwegian transmission system operator, Statnett.



# Chapter 3

## Thermal modeling of power cables

First in this theory chapter, an introduction to the conventional steady-state and transient rating methods used by utilities is given. Secondly, the method to establish a thermal equivalent cable circuit for temperature calculations is explained. Which includes calculations of the thermal resistances and heat capacitances that are required to calculate the thermal response. Further, the equations needed for transient temperature calculations, based on temperature rise in the internal parts of the cable and environmental impact, are given. Lastly, this chapter describes the principle of superposition, which is utilized to calculate total temperature rise for load profiles consisting of multiple current steps.

This thesis is limited to calculating transient temperature rise for directly buried cables. However, some buried cable systems also have sections where the cable is laying in air, such as pipe cables. Therefore, equations for calculating thermal resistance for pipe type cables are also included. The cable rating book by Anders [15] has been of great help in describing the transient calculation method given in IEC 60853 [57].

Furthermore, the cable used for the simulations in this thesis is a single-core XLPE insulated direct current (DC) cable. Therefore, equations describing screen losses and dielectric losses (which are not present for this cable type), are not included in this theory chapter. For other cable types however, these losses may affect the rating of the cable and should be considered in rating calculations. Equations and calculation methods of these types of losses may be found in [15].

Moreover, the equations presented in this chapter do not take account for mutual heating of a group of cables, as it is assumed a cable circuit only consisting of one single-core cable. Mutual heating of nearby cables reduces the ampacity of the cables and must be taken into account in rating computations for cable circuits consisting of more than one

cable. Methods taking the presence of more than one cable into account are described in Anders [15] and the IEC standards [10, 57].

The properties of the cable environment may change due to variations in moisture content in the surrounding soil caused by moisture migration during heavy loading. As a result of moisture migration, a dried out zone may develop around the cable, in which the thermal conductivity is reduced. This can in turn lead to damage of the cable insulation due to increased temperatures [58]. In Anders [15], equations describing the effect of moisture migration in steady-state ampacity ratings is presented. Computation examples show that a reduction in cable ampacity by several percent can be expected. However, less information of the behavior of moisture migration under cyclic loading is obtained. The complicated matter of moisture migration during transient loads is therefore not included in this thesis and not covered in this theory section.

### **3.1 Conventional cable rating standards**

Commonly used modeling approaches for cables are often based on conventional IEC standards for rating of power cables. For transient temperature calculations, the IEC 60853 standard is widely used, while IEC 60287 is used for steady-state temperature calculations [10, 57].

The "IEC 60853 - Calculation of the cyclic and emergency current rating of cables" is divided into three parts. The first part describes the cyclic rating factor for cables up to and including 18/30(36) kV, while the second part covers the cyclic rating factor of cables greater than 18/30(36) kV and emergency ratings for all voltages. The third part of the standard includes partial drying of the soil [57, 59, 60].

For steady-state rating calculations, the "IEC 60287 - Calculation of the continuous current rating of cables (100% load factor)", is used. By the term "steady-state", it means continuous constant current (100% load factor) to obtain asymptotically the maximum permitted conductor temperature, while ambient conditions are assumed constant. The reason to include the steady-state current rating standard is that the thermal equivalent representation, boundary conditions and calculations of thermal resistivities and losses are equal for both rating methods and obtained from IEC 60287.

### **3.2 Establishing the cable thermal equivalent**

To tackle the heat conduction problem in power cables, the fundamental similarity between the heat flow due to temperature differences between the current carrying conductor and its surroundings and the flow of electrical current caused by difference of potential, is used. By dividing the cable into a number of volumes represented by their thermal resistance



and heat capacitance, a lumped parameter method is used to solve differential equations in the heat conduction problem. The thermal network is analogous to the electrical networks in which temperatures are equivalent to voltages and heat flows to currents, while thermal resistance and heat capacitance are equivalent to electrical resistance and capacitance. The lumped parameter representation of the thermal network is a simplified way to analyze complex cable constructions and is widely used for thermal analysis [15].

### 3.2.1 Thermal resistance of the cable parts and surrounding soil

All non-conductive materials in the cable will impede heat flow away from the cable due to their thermal resistance. By taking advantage of the circular geometry of the cable layers, the thermal resistance of these parts may be calculated. For all cylindrical parts of a single-core cable, the thermal resistance per unit length is calculated from equation 3.1 [10]. The index  $i$  can be 1, 2 or 3 referring to the insulation, metallic screen and sheath, respectively. However, the thermal resistance of the metallic screen ( $T_2$ ) can be neglected in rating computations due to the low thermal resistivity [10].

$$T_i = \frac{\rho_i}{2\pi} \ln \left( 1 + \frac{2t_i}{D_i} \right) \quad (3.1)$$

In which:

- $\rho_i$  = thermal resistivity of material in layer  $i$  [K·m/W]
- $t_i$  = thickness of layer  $i$  [mm]
- $D_i$  = diameter beneath layer  $i$  [mm]

The ampacity rating of cables depends to a large extent on the thermal resistance of the surroundings. For buried cables, this resistance accounts for more than 70% of the temperature rise of the conductor, while it has less effect on cables in air [58].

For directly buried cables laying in a uniform soil where the depth of burial is much greater than the cable diameter, a short form of the Kennelly formula (equation 3.2) can be used to calculate the thermal resistance of the soil [15].

$$T_4 = \frac{\rho_{soil}}{2\pi} \ln \left( \frac{4L}{D_e} \right) \quad (3.2)$$

Where:

- $\rho_{soil}$  = soil thermal resistivity [K·m/W]
- $L$  = cable burial depth [mm]
- $D_e$  = external diameter of the cable [mm]

For cables laying in air ducts, the external thermal resistance consists of three parts:

1. Thermal resistance of the air between the cable surface and the duct internal surface,  $T_4'$
2. Thermal resistance of the duct itself,  $T_4''$
3. External thermal resistance of the duct,  $T_4'''$

The total external thermal resistance to be used in rating equation will be the sum of the three individual parts: [15]

$$T_4 = T_4' + T_4'' + T_4'''$$

The total heat loss from the cable surface is equal to the sum of the conductive heat transfer rate in the cable surroundings and the natural convection and thermal radiation heat transfer rate between the cable outside surface and its surroundings. By taking this heat emanating from the cable and the temperature difference between the cable surface and inner duct into account,  $T_4'$  is calculated from equation 3.3 [15].

$$T_4' = \frac{\theta_s - \theta_w}{W_{conv,s} + W_{cond} + W_{rad,s-w}} \quad (3.3)$$

Where:

- $W_{conv,s}$  = natural convection heat transfer rate between the cable outside surface and its surroundings [W/m]
- $W_{cond}$  = conductive heat transfer rate in the cable surroundings [W/m]
- $W_{rad,s-w}$  = thermal radiation heat transfer rate between the duct inner surface and the cable outside surface [W/m]
- $\theta_s$  = cable sheath temperature [°C]
- $\theta_w$  = duct inner surface temperature [°C]

Solving equation 3.3 has traditionally been a complicated task since the value of  $T_4'$  depends on the unknown temperatures  $\theta_s$  and  $\theta_w$ . The heat transfer rates from the cable are also dependent on these temperatures. Therefore, several iterations are required to solve the equation for  $T_4'$  and the absence of digital computers made it necessary to simplify the equation. However, with simple temperature measurements of the required temperatures (such as DTS monitoring of the cable surface temperature), solving the thermal resistance of the air between the cable surface and the duct internal surface is fairly doable.

The thermal resistance of the duct itself,  $T_4''$ , is dependent on the shape of the duct. For a circular duct (pipe), the thermal resistance is calculated by a direct application of equation 3.1. External thermal resistance of the duct,  $T_4'''$ , is obtained in the same way as for a buried cable [15].

### 3.2.2 Heat capacitance of the cable parts

For dynamic rating problems, the material's ability to store heat must be considered. A lumped capacitance method is applied to solve heat equations analytically for cable rating computations. The heat capacitance per unit length of a material can be written as equation 3.4 [15].

$$Q = A \cdot C_v \quad (3.4)$$

In which:

- $Q$  = heat capacitance of material [J/K·m]  
 $A$  = area of material [m<sup>2</sup>]  
 $C_v$  = volumetric heat capacity of material [J/K·m<sup>3</sup>]

The heat capacitance for a coaxial configuration, such the cable insulation and sheath, is established from equation 3.5.

$$Q = \frac{\pi}{4} (D_{ex}^2 - D_{in}^2) \cdot C_v \quad (3.5)$$

Where  $D_{in}$  and  $D_{ex}$  is the internal diameter and external diameter, respectively.

However, for the insulation (and other dielectrics), heat capacity is not a linear function of the thickness. To improve the accuracy of the lumped parameter approximation, Van Wormer developed a method for allocating the heat capacity between the conductor and screen. The heat capacity of the insulation is divided into a portion  $pQ_{ins}$  placed at the conductor and a portion  $(1 - p)Q_{ins}$  at the screen, where  $p$  is the Van Wormer Coefficient given by: [15]

$$p = \frac{1}{2 \ln\left(\frac{D_{ins}}{D_c}\right)} - \frac{1}{\left(\frac{D_{ins}}{D_c}\right)^2 - 1} \quad (3.6)$$

In which  $D_c$  and  $D_{ins}$  is the internal insulation diameter (conductor diameter) and external insulation diameter, respectively. The Van Wormer Coefficient for the sheath is calculated in the same way:

$$p' = \frac{1}{2 \ln\left(\frac{D_e}{D_s}\right)} - \frac{1}{\left(\frac{D_e}{D_s}\right)^2 - 1} \quad (3.7)$$

In which  $D_s$  and  $D_e$  is the internal sheath diameter and cable diameter, respectively.

### 3.2.3 Resulting thermal equivalent

Figure 3.1 shows the cross section of a typical single-core DC cable consisting of a conductor, insulation, screen and sheath. The thermal equivalent circuit for this cable is presented in figure 3.2. For directly buried cables, the equivalent circuit is considered to extend as far as the cable sheath.

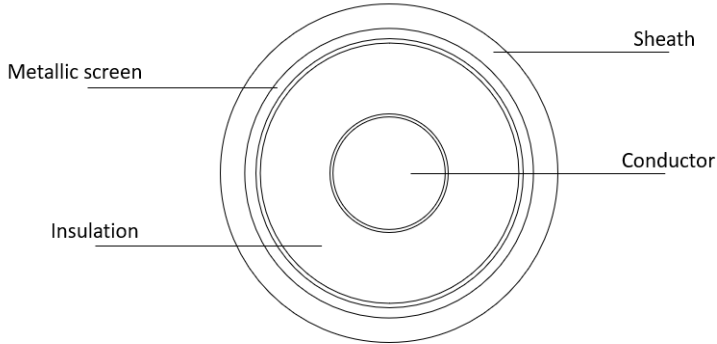


**Figure 3.1:** Cross section of the single-core power cable with a conductor, insulation layer, metallic screen and protective sheath.

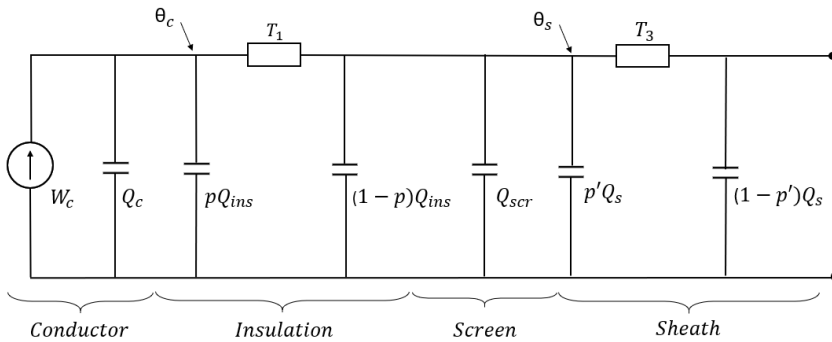


**Figure 3.2:** Transient thermal equivalent of the power cable in figure 3.1.

Where the parameter designation is as following:

- $Q_c$  = heat capacitance of the conductor [J/mK]
- $Q_{ins}$  = heat capacitance of the insulation [J/K·m]
- $Q_{scr}$  = heat capacitance of the screen [J/K·m]
- $Q_s$  = heat capacitance of the sheath [J/K·m]
- $W_c$  = conductor losses per meter cable [W/m]

The thermal resistances  $T_1$  and  $T_3$  are described in section 3.2.1, while the Van Wormer Coefficients  $p$  and  $p'$  are described in section 3.2.2.

Generally, the thermal equivalent circuit of a cable should include representations of screen loss and the dielectric loss. However, for a DC cable there are no currents flowing in the metallic screen, thus no screen losses. The heat produced in the insulation material due to alternating current results in dielectric loss. For DC cables however, this type of loss is not present. Moreover, in XLPE insulated cables, the low thermal resistivity of the insulation results in low dielectric loss and may also be neglected for low and medium voltage XLPE alternating current (AC) cables [15].

### 3.3 Transient cable conditions

To calculate the total temperature rise of a cable, the IEC standard divides the temperature rise into one portion caused by the internal parts of the cable, and one portion caused by the surroundings. The temperature rise due to the internal parts is modeled based on the thermal equivalent in figure 3.2, while the temperature rise due to the cable environment can be evaluated by representing the cable as a line source in an infinite homogeneous medium [51]. The sum of these individually calculated responses is the total temperature rise of the cable above ambient.

#### 3.3.1 Temperature rise in the internal parts of the cable

To solve the linear network in figure 3.2, a determination of the expression for the response function (temperature rise above the cable surface) caused by a forcing function (conductor heat loss), is required. The determination of the response function is accomplished by utilizing the transfer function (equation 3.8) of the thermal equivalent. The transfer function can be solved for all loops of the network in figure 3.2, thus calculating the temperature at any part (node) of the cable. The polynomials  $Y(s)$  and  $X(s)$  depend on the number of loops in the network [15].

$$H(s) = \frac{Y(s)}{X(s)} \quad (3.8)$$

The temperature of each node in the network may be calculated by the time response obtained by the transfer function as in equation 3.9 [15].

$$\theta_m = W_c \sum_{j=1}^n T_{mj} (1 - e^{P_j t}) \quad (3.9)$$

In which:

$\theta_m(t)$	=	temperature rise at node $m$ at time $t$ [ $^{\circ}\text{C}$ ]
$W_c$	=	conductor losses per meter cable [ $\text{W/m}$ ]
$T_{mj}$	=	coefficient from thermal equivalent
$P_j$	=	time constants determined from the poles of the transfer function, [ $\text{s}^{-1}$ ]
$t$	=	time from the beginning of the step [ $\text{s}$ ]
$n$	=	number of loops in the network
$m$	=	node index
$j$	=	index from 1 to $n$

Further, the coefficients  $T_{mj}$  and the time constants  $P_j$  are obtained from the poles and zeros of the transfer function. The coefficients  $T_{mj}$  are given by equation 3.10 [15].

$$T_{mj} = -\frac{x_{(n-m)m}}{y_n} \frac{\prod_{k=1}^{n-m} (Z_{km} - P_j)}{P_j \prod_{\substack{k=1 \\ k \neq j}}^n (P_k - P_j)} \quad (3.10)$$

Where:

$x_{(n-m)m}$	=	coefficient of the numerator equation of the transfer function
$y_n$	=	first coefficient of the denominator equation of the transfer function
$Z_{km}$	=	zeros of the transfer function
$P_j, P_k$	=	poles of the transfer function
$k$	=	index from 1 to $n$ , $k \neq j$

### 3.3.2 Cable environment impact on the temperature rise

The hypothesis of Kennelly, which assumes the soil surface to be an isotherm, can be used to calculate the temperature rise caused by the surroundings. By utilizing this assumption in conjunction with representing the cable as a line source in an infinite homogeneous medium, the temperature rise caused by the surroundings can be calculated from equation 3.11 [51].

$$\theta_e = W_c \frac{\rho_{soil}}{4\pi} \left[ -Ei\left(-\frac{D_e^2}{16\delta t}\right) + Ei\left(-\frac{L^2}{\delta t}\right) \right] \quad (3.11)$$

Where  $\rho_{soil}$  and  $\delta$  is the thermal resistivity and diffusivity of the soil, respectively, while the parameters  $L$  and  $D_e$  are described earlier in section 3.2.1. The exponential integral  $-Ei(-x)$  can be developed in the series:

$$-Ei(-x) = -0577 - \ln(x) + x - \frac{x^2}{2 \cdot 2!} + \frac{x^3}{3 \cdot 3!} \cdots \quad (3.12)$$

The diffusivity of the soil will vary with density, moisture content and thermal conductivity. In most cases, diffusivity of the soil is not known exactly and the value of  $5 \cdot 10^{-7} \text{ m}^2/\text{s}$  is often a good approximation. This value is based on a moisture content of 7% and a soil thermal conductivity of  $1 \text{ W/K}\cdot\text{m}$  [15]. However, if the density, heat capacity and thermal conductivity of a material is known, the diffusivity may be calculated from equation 3.13 [61].

$$\delta = \frac{\lambda_{soil}}{d_{soil} \cdot C_{p,soil}} \quad (3.13)$$

In which:

- $\lambda_{soil}$  = thermal conductivity of the soil [ $\text{W/K}\cdot\text{m}$ ]
- $d_{soil}$  = density of soil [ $\text{Kg/m}^3$ ]
- $C_{p,soil}$  = heat capacity of soil at constant pressure [ $\text{J/kg}\cdot\text{K}$ ]

### 3.3.3 Resulting temperature rise

The total temperature rise of the cable above ambient is a combination of the temperature rise in the internal parts of the cable and the temperature rise caused by the surroundings, given by:

$$\theta(t) = \theta_m(t) + \gamma(t) \cdot \theta_e(t) \quad (3.14)$$

In which  $\theta_m(t)$  is and  $\theta_e(t)$  are described in section 3.3.1 and 3.3.2, respectively and  $\gamma(t)$  is the attainment factor for the transient temperature rise between the cable and its surroundings.

The attainment factor is used to take into account the heat developed in the cable during early parts of a transient, as the environmental temperature rise effect is not felt immediately [51]. The attainment factor can be described as the temperature rise across the cable at time  $t$  divided by the steady-state temperature rise across the cable.

### 3.3.4 Temperature dependent resistance of the conductor

The electrical resistance of metallic parts of the cable changes with temperature, which in turn will affect the total heat loss. Therefore, these changes should be taken into account when computing conductor losses. The following equation is used to calculate the temperature dependent conductor loss: [15]

$$W_c = I^2 R_\theta \quad (3.15)$$

In which  $I$  is the cable's load carrying current and  $R_\theta$  is the temperature dependent conductor resistance: [62]

$$R_\theta = R_{20}[1 + \alpha_{cu}(\theta_c - 20)] = \frac{\rho_{c,20} \cdot l}{A}[1 + \alpha_{cu}(\theta_c - 20)] \quad (3.16)$$

Where:

- $\rho_{c,20}$  = conductor resistivity at 20 °C [ $\Omega \cdot m$ ]
- $R_{20}$  = conductor resistance at 20 °C [ $\Omega$ ]
- $A_c$  = conductor area [ $m^2$ ]
- $l$  = length [m]
- $\alpha_{cu}$  = temperature coefficient (0.0039 for copper [10]) [ $1/K$ ]
- $\theta_c$  = conductor temperature [ $^{\circ}C$ ]

### 3.3.5 Transient temperature rise under variable loading (Superposition principle)

The previously described equations are valid for a single step-current as input. To perform computations for variable loading, a load curve must be divided into a series of steps of constant magnitude. By utilizing the principle of superposition, the final temperature rise, as a function of time, can be calculated [15]. Figure 3.3 illustrates the principle of superposition and the temperature rise due to a two step current (one step up and one step down).

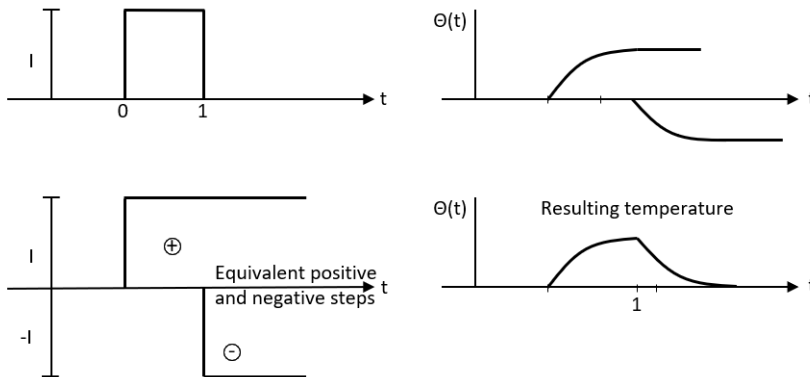


**Figure 3.3:** Illustration of the principle of superposition to calculate the resulting temperature rise due to two step current (one step up and one step down).

It can be seen from figure 3.3 that by the total temperature rise due to a multi-step current load is obtained by adding the movements towards a hypothetical steady-state temperature for all current steps. Mathematically, the total temperature rise can be modeled in terms of a summation of exponential expressions describing the transient temperature rise caused by a step current change [51].



# Chapter 4

## Thermal aging of cable insulation

The purpose of this theory chapter is to deal with aging mechanisms in the cable insulation related to increased thermal stress due to overloading. However, the cable is also subjected to other aging mechanisms, such as mechanical stress and electrical stress. The connection between cable lifetime and the stress the cable is exposed to, is therefore complicated. This thesis is however limited to evaluating how the extra aging increased temperatures, caused by overloading, will inflict on the insulation material. Therefore, only the thermal aging mechanisms are covered in this chapter. Explanations and more detailed treatment of the other mentioned aging mechanisms can be found elsewhere in Papadopulos [63], Dissado and Fothergill [64] and Montanari et al. [65].

Higher operating temperatures result in increased thermal stress that ages the cable faster than more moderate operating temperatures would. In a report from 1930, Montsinger [66] studied the relationship between temperature and time to failure of insulation material. The relationship Montsinger found, stated that a temperature increase of 8 - 10 °C results in a doubling of the aging rate.

Based on the empirical relationship that Montsinger described, researchers have tried to infer the aging due to temperature. Dakin [67] proposed in 1948 a theory suggesting that the rate of thermal aging is caused by the chemical reactions due to increased temperature. As thermally induced aging has its origin in chemical changes of the insulation material, the main emphasis in this chapter has been on chemical degradation.

## 4.1 Thermal aging due to chemical degradation

Chemical degradation is caused by the formation of free polymer radicals that are chemically reactive. These radicals cause three main degradation phenomena, namely: chain scission and cross-linking net formation by chain reactions, and oxidation by absorbed oxygen [64].

Oxidation is often the most dominant form of degradation of insulation material. By introducing acid groups into the polymer, the conductivity increases. A splitting of the polymer chains also occurs, leading to decreased tensile strength. The cross-linking will result in an increasing hardness of the polymer, but decrease the bending and stretching strength, making it more brittle. Degradation by chain scission is purely thermal and is, in short, the phenomena of polymer chains breaking into smaller units. This reaction is much slower than for example oxidation, but at elevated temperatures, degradation is likely to be caused by chain scission [67].

To terminate the forming of free radicals in the polymer, primary antioxidants are added to the insulation material. The primary antioxidants act as free radical scavengers, thus retarding the chemical degradation by forming stable compounds with the free radicals [68].

According to Dakin's theory developed in 1948, elevated temperatures will increase the rate of chemical reactions in the polymer [67]. Thus, the relationship between the temperature and degradation rate has the same form as the equation for the chemical reaction rate [65]. Therefore, the thermal aging of the insulation can be assumed proportional to the rate of chemical reactions, known as the Arrhenius law given in equation 4.1 [7, 69].

$$r = r' \cdot e^{-\frac{w}{k_B \theta}} \quad (4.1)$$

In which:

- $r$  = rate of chemical reaction (probability that a chemical reaction will occur within one unit of time)
- $r'$  = a constant
- $w$  = activation energy of the main thermal degradation reaction [eV]
- $\theta$  = absolute operating temperature [K]
- $k_B$  = Boltzmann's constant,  $0.8617 \cdot 10^{-4}$  [eV/K]

Further, equation 4.1 may be rewritten to describe the thermal lifetime:

$$L(\theta) = L_0 \cdot e^{-\frac{w}{k_B \theta}} \quad (4.2)$$

In which  $L_0$  is the thermal insulation lifetime at reference temperature ( $\theta_0$ ).

The Arrhenius model has been widely used for accelerated aging tests, but the model can also be used to assess the natural aging of cables. A typical way of representing the Arrhenius equation 4.2 is by an Arrhenius plot, shown in figure 4.1. The model gives rise to a slope of  $-\frac{w}{k_B}$ , which enables the extrapolation from test values at elevated temperatures to evaluate the lifetime at service temperatures.

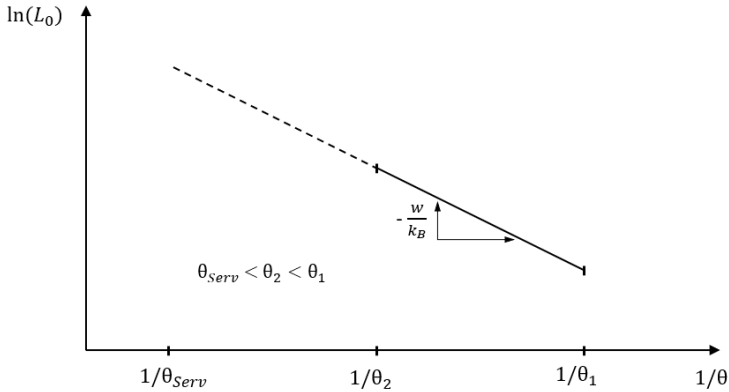


**Figure 4.1:** Arrhenius plot used for estimating cable lifetime at service temperatures.

However, the Arrhenius model may not hold true for low thermal stresses. By experience in Mazzanti and Montanari [70], a thermal threshold for XLPE insulated cables was found. By thermal threshold it is meant that at a certain temperature, the thermal aging practically ceases and material lifetime tends to be so long it can be considered infinite. In practice, the aging rate at such low stress is so small that operating at these temperatures will not affect the cable lifetime.

## 4.2 Thermal degradation over an overload period

If a power cable is subjected to intermittent overloading, the conductor temperature will exceed temperatures encountered during normal operation. By applying conductor temperatures calculated from the given overloading profile to an Arrhenius model, the additional aging may be assessed. The total aging during an overload period can be estimated by utilizing corresponding thermal aging rates for the calculated temperature profile. In which the aging rate is the reciprocal lifetime [8].

By dividing the temperature profile of an overloading period into  $K$  intervals, the aging rate and time period of each interval may be used to calculate the lifetime consumption (aging) of that interval. The total lifetime consumption caused by thermal aging during

the whole overloading period is given by Miner's cumulative aging theory: [71]

$$L_f = \sum_{i=1}^K R_{a,i}(\theta) \cdot t_{D,i} \quad (4.3)$$

In which  $R_{a,i}(\theta)$  is the aging rate for the specific temperature at the  $i^{th}$  interval and  $t_{D,i}$  is the time period of which the aging rate is acting.  $L_f$  is the total loss of life (in percentage of expected lifetime) for the whole overload period. For example, if  $L_f = 50\%$ , it means that half of the total cable lifetime is consumed.

# Chapter 5

## Analytical and numerical thermal model of a single-core XLPE cable

The following chapter describes how the thermal modeling was conducted both from an analytical perspective based on IEC standards for cable ratings and numerical with COMSOL Multiphysics. Further, this chapter proposes some overloading case examples to investigate for how long and to what extent the given cable may be overloaded for different scenarios. It was also estimated how these overload scenarios would affect the cable lifetime due to extra aging caused by higher operating temperatures.

The cable chosen for the transient temperature calculations was a single core 10 kV XLPE cable, based on the cable dimension for Model Cable No. 1 in Appendix A in Anders [15]. Figure 5.1 shows the cross-section of the cable model, while cable dimensions are recalled in table 5.1. Burial depth of 1 meter was used for all simulations, while soil temperature at burial depth was set to 15 °C.

The maximum rated current under steady-state conditions for the cable in figure 5.1 is, according to the IEC 60287 standard, 1000 A. Which is the current that would cause 90 °C conductor temperature after being applied until steady conditions. However, the conductor cross section area is often oversized to take into account laying formation and environmental conditions. In addition, increased future electricity demand makes it reasonable to use larger conductors. Permitted loading in a power system may be based on the ampacity of other components, rather than the cable itself.

Therefore, henceforth in this thesis, the term rated current of the cable is meant to represent rated current of a whole power system and not the maximum rated current of the cable itself. Consequently, the rated current was chosen as a lower value than the maximum rated current calculated from the IEC standard for continuous loading. A reasonable value

was chosen as 30% under maximum rated current for the cable itself. Thus, rated current was set to 700 A.

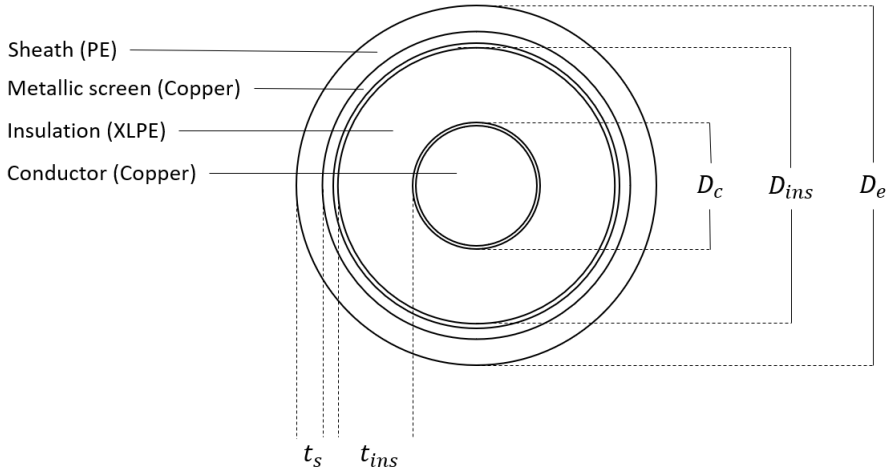


**Figure 5.1:** Cross section of the single core cable used in the modeling.

**Table 5.1:** Data for a single core 10 kV cable [15].

Conductor diameter ( $D_c$ )	20.5	[mm]
Insulation diameter ( $D_{ins}$ )	30.1	[mm]
Cable diameter ( $D_e$ )	35.8	[mm]
Insulation thickness ( $t_{ins}$ )	4.9	[mm]
Sheath thickness ( $t_s$ )	2.3	[mm]

The cable is constructed of a copper conductor, XLPE insulation, copper screen and a protective polyethylene (PE) sheath. Between the conductor and the insulation and between the insulation and the screen, a thin semiconductive layer is present to equalize the electrical stress on the cable insulation. However, due to similar properties, this layer is treated like an insulation layer and therefore included in the XLPE thickness in the calculations.

## 5.1 Analytical modeling based on the IEC standards

Based on the conventional standards IEC 60853 for cyclic loading and IEC 60827 for continuous loading, a method to calculate transient conductor and sheath temperatures was carried out. A MATLAB program was conducted in order to calculate the developed algorithm based on the IEC standards. The MATLAB source code can be found in Appendix D.

First, the material properties of the cable parts and the surrounding soil were specified. Thermal resistivity and specific heat for XLPE and PE was found in [15], while for copper, material properties were obtained from the Materials library in COMSOL. All material properties used in the calculations are recalled in table 5.2.

**Table 5.2:** Material properties of the cable parts and the surrounding soil used in the analytical modeling approach.

	Copper (conductor and screen)	XLPE/PE (insulation and sheath)	Surrounding soil
Thermal resistivity [K·m/W]*	-	3.5	1
Volumetric heat capacity ( $\cdot 10^6$ ) [J/K·m <sup>3</sup> ]*	3.45	2.4	-

\* At 20 °C

The thermal equivalent for the single-core cable of the same type as shown in figure 5.1, was conducted in section 3.2.3 and is for convenience recalled in figure 5.2.

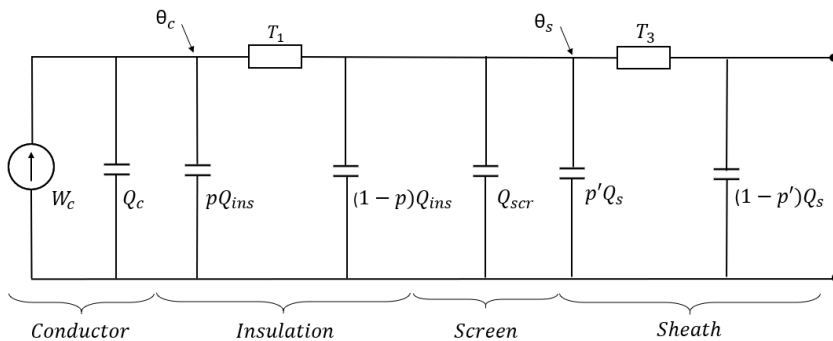


**Figure 5.2:** Transient thermal equivalent of cable in figure 5.1 directly buried.

Based on the material properties in table 5.2 and the cable dimensions recalled in table 5.1, the lumped parameters in the thermal equivalent circuit in 5.2 were calculated from the equations described in section 3.2.1 and 3.2.2. The calculated values can be seen in table 5.3.

**Table 5.3:** Lumped parameters calculated based on IEC 60853.

$Q_{scr}$	182.71	[J/K·m]	$T_1$	0.2137	[K·m/W]
$Q_s$	580.94	[J/K·m]	$T_2$	0.0716	[K·m/W]
$Q_c$	1035	[J/K·m]	$p$	0.4366	
$Q_{ins}$	915.64	[J/K·m]	$p'$	0.4771	

The transient thermal equivalent circuit of the cable in figure 5.2 may be represented as a network composed of two loops, as in figure 5.3. By reducing the network to a two-loop equivalent, computations for the transient response of a cable to variable load may be done for each node (e.g. conductor temperature,  $\theta_c$ , or sheath temperature,  $\theta_s$ ). The first section of the two-loop equivalent includes the thermal capacitance of the conductor, the first portion of the insulation capacitance and the thermal resistance of the insulation. The second section of the circuit includes the remaining thermal resistances and capacitances of the cable components.

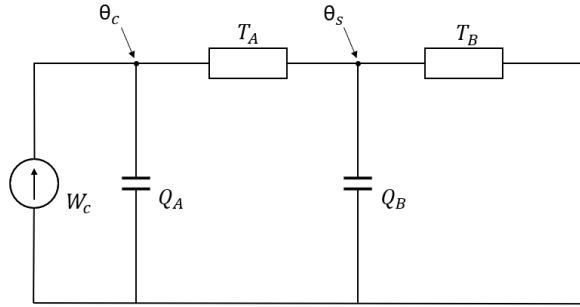


**Figure 5.3:** Two-loop thermal equivalent for temperature calculations.

Where:

$$\begin{aligned}
 T_A &= T_1 \\
 T_B &= T_3 \\
 Q_A &= Q_c + pQ_{ins} \\
 Q_B &= (1 - p)Q_{ins} + Q_{scr} + p'Q_s
 \end{aligned}$$

Values of the new thermal resistances and heat capacitances in figure 5.3 are shown in table 5.4.

**Table 5.4:** Calculated values of the thermal resistances and heat capacitances in figure 5.3.

$T_A$	0.2137	[K·m/W]
$T_B$	0.0716	[K·m/W]
$Q_A$	1434.8	[J/K·m]
$Q_B$	975.75	[J/K·m]



### 5.1.1 Conductor temperature rise

Based on a computation algorithm shown in [15], the time dependent solution for the conductor temperature rise was calculated. The transfer function for the conductor node ( $\theta_c$ ) of the network in figure 5.3 is given by equation 5.1.

$$H_c(s) = \frac{\theta_c}{W_c} = Z_{tot} \quad (5.1)$$

In which  $Z_{tot}$  is the impedance "downstream" of the conductor node, which equals the total impedance of the network:

$$Z_{tot} = \frac{1}{sQ_A + \frac{1}{T_A + \frac{1}{sQ_B + \frac{1}{T_B}}}} \quad (5.2)$$

Further, by solving the complex fraction of 5.2, the total transfer function for the conductor node is given in equation 5.3. The derivation of the transfer function is given in Appendix A.

$$H_c(s) = \frac{T_A + T_B + sT_A T_B Q_B}{1 + s(T_A Q_A + T_B Q_A + T_B Q_B) + s^2 T_A T_B Q_A Q_B} \quad (5.3)$$

The zeros and poles of the transfer function (5.3) are given by:

$$Z_{11} = -\frac{T_A + T_B}{T_A T_B Q_B}, \quad P_1 = -a, \quad P_2 = -b \quad (5.4)$$

Where:

$$a = \frac{M_0 + \sqrt{M_0^2 - N_0}}{N_0}, \quad b = \frac{M_0 - \sqrt{M_0^2 - N_0}}{N_0} \quad (5.5)$$

In which:

$$M_0 = \frac{1}{2}(T_A Q_A + T_B Q_A + T_B Q_B), \quad N_0 = T_A T_B Q_A Q_B \quad (5.6)$$

The coefficients of the numerator and the denominator of the transfer function are shown in equation 5.7.

$$x_{(n-m)m} = x_{12} = T_A T_B Q_B, \quad y_n = y_2 = T_A T_B Q_A Q_B \quad (5.7)$$

Further, the coefficients  $T_{11}$  and  $T_{12}$  are obtained by equation 3.10. The derivation of equations for the coefficient  $T_{11}$  and  $T_{12}$  is shown in appendix A.

$$T_{11} = \frac{1}{a-b} \left[ \frac{1}{Q_A} - b(T_A + T_B) \right] \quad (5.8)$$

$$T_{12} = \frac{1}{b-a} \left[ \frac{1}{Q_A} - a(T_A + T_B) \right] \quad (5.9)$$

Values of all the calculated parameters needed to obtain the total temperature rise of the conductor based on the above equations are recalled in table 5.5.

**Table 5.5:** Calculated parameters from equation 5.4 - 5.9 used in the conductor temperature rise calculation.

$a$	0.02	$[s^{-1}]$	$N_0$	21426	$[s^2]$
$b$	0.0023	$[s^{-1}]$	$T_{11}$	0.0018	$[K \cdot m/W]$
$M_0$	239.64	$[s]$	$T_{12}$	0.2835	$[K \cdot m/W]$

The temperature rise of the conductor node is calculated from the time response obtained by the transfer function 5.3, as shown in section 3.3.1:

$$\theta_c(t) = W_c [T_{11}(1 - e^{-at}) + T_{12}(1 - e^{-bt})] \quad (5.10)$$

Finally, by inserting values, the conductor temperature rise above cable surface due to a step function input based on the thermal equivalent may thus be described as:

$$\theta_c(t) = W_c [0.0018(1 - e^{-0.02t}) + 0.2835(1 - e^{-0.0023t})]$$

Where  $W_c$  is the power loss per unit length in the conductor based on the conductor temperature attained, which is calculated for each time interval. Equations to calculate the conductor loss based on the temperature dependency of the resistance are shown in section 3.3.4, but are for convenience recalled in equation 5.11 and 5.12.

$$W_c = I^2 R_\theta \quad (5.11)$$

In which  $I$  is the cable's load carrying current and  $R_\theta$  is the temperature dependent conductor resistance:

$$R_\theta = R_{20} [1 + \alpha_{cu}(\theta - 20)] = \frac{\rho_{c,20} \cdot l}{A} [1 + \alpha_{cu}(\theta - 20)] \quad (5.12)$$

Data used in the simulations for the parameters above is shown in table 5.6.

**Table 5.6:** Data for different parameters used in calculation of the temperature dependent conductor resistance.

Conductor resistivity ( $\rho_{c,20}$ ) at 20 °C [10]	$1.72 \cdot 10^{-8}$	$[\Omega \cdot m]$
Temperature coefficient copper ( $\alpha_{cu}$ ) [10]	0.0039	$[1/K]$
Conductor area ( $A$ )	$300 \cdot 10^{-6}$	$[m^2]$
Length ( $l$ )	1	$[m]$

The change in resistance with increasing temperature for a 300 mm<sup>2</sup> copper conductor is shown in figure 5.4.

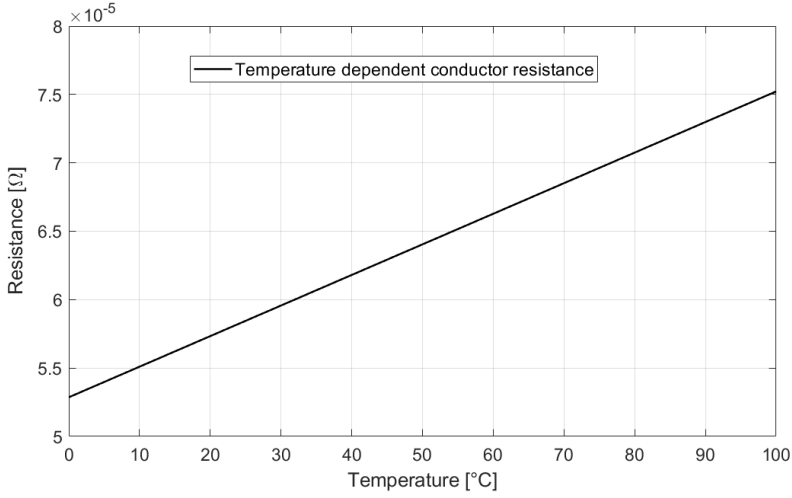


**Figure 5.4:** Temperature dependent resistance for a 300 mm<sup>2</sup> copper conductor.

### 5.1.2 Sheath temperature rise

In addition to calculating the conductor temperature rise, the equivalent network in 5.3 may also be solved with respect to  $\theta_s$ , thus providing the sheath temperature rise as a function of time. This temperature is of interest since sheath temperatures can be measured by temperature monitoring equipment. The sheath temperature is therefore in reality a measurable quantity, while the conductor temperature must be predicted.

From the two-loop equivalent in figure 5.3, the transfer function from the sheath node may be written as equation 5.13.

$$H_s(s) = \frac{\theta_s}{W_c} = \frac{Z_b}{1 + sQ_A(T_A + Z_b)} \quad (5.13)$$

In which  $Z_b$  is the total impedance "downstream" of the sheath node, given by:

$$Z_b = \frac{1}{sQ_B + \frac{1}{T_B}} \quad (5.14)$$

Solving the complex fraction in equation 5.13, the transfer function of the second node ( $\theta_s$ ) is given by equation 5.15. For full derivation of the transfer function, see appendix A.

$$H_s(s) = \frac{T_B}{1 + s(T_AQ_A + T_BQ_A + T_BQ_B) + s^2T_AT_BQ_AQ_B} \quad (5.15)$$

The time constants as well as the poles are equal to the ones obtained in section 5.1.1, while there are no zeros for the transfer function for the sheath node. The coefficients of the numerator and the denominator of the transfer function are shown in equation 5.16.

$$x_{(n-i)i} = x_2 = T_B, \quad y_n = y_2 = T_A T_B Q_A Q_B \quad (5.16)$$

Thus, the coefficients  $T_{21}$  and  $T_{22}$  are obtained from equation 3.10. For full derivation of equation 5.17 and 5.18, please refer to appendix A.

$$T_{21} = -\frac{T_B}{T_A T_B Q_A Q_B} \frac{a}{-a(-b+a)} = \frac{T_B \cdot ab}{a-b} \quad (5.17)$$

$$T_{22} = -\frac{T_B}{T_A T_B Q_A Q_B} \frac{a}{-b(-a+b)} = \frac{T_B \cdot a^2}{a-b^2} \quad (5.18)$$

Values for the coefficients  $T_{21}$  and  $T_{22}$  are given in table 5.7.

**Table 5.7:** Values of coefficients  $T_{21}$  and  $T_{22}$  in calculations of sheath temperature rise.

$T_{21}$	0.00019	[K·m/W]	$T_{22}$	0.0014	[K·m/W]
----------	---------	---------	----------	--------	---------

The temperature rise of the sheath node is calculated from the time response obtained by the transfer function (equation 5.15):

$$\theta_s(t) = W_c [T_{21}(1 - e^{-at}) + T_{22}(1 - e^{-bt})] \quad (5.19)$$

Further, when inserting the calculated values for the coefficients, the sheath temperature rise as a function of time may be written as:

$$\theta_s(t) = W_c [0.00019(1 - e^{-0.02t}) + 0.0014(1 - e^{-0.0023t})]$$

In which  $W_c$  is the power loss per unit length in the conductor, described in section 5.1.1.

### 5.1.3 Cable environment impact on the temperature rise

By assuming the cable is a line source in an infinite homogeneous medium and that the earth surface is an isotherm, the Kennelly hypothesis can be utilized as described in section 3.3.2. Thus, equations 3.11 and 3.12 can be used to describe the influence of soil. For the diffusivity of soil, an approximate value of  $5 \cdot 10^{-7} \text{ m}^2/\text{s}$  was chosen.

However, the exponential integral  $-Ei(-x)$  is rather complex to solve and the execution time in MATLAB was too long for many evaluation steps. Therefore, the following rational approximation, derived in the IEC 60853 standard [57], was used:

For  $0 \leq x \leq 1$ :

$$-Ei(-x) = -\ln(x) + \sum_{i=0}^5 a_i x^i$$

Values for  $a_i$  may be found in Appendix B.

For  $0 < x < 8$ :

$$-Ei(-x) = \frac{1}{xe^x} \left[ \frac{x^2 + a_1x + a_2}{x^2 + b_1x + b_2} \right]$$

Where the values of  $a_1$ ,  $a_2$ ,  $b_1$  and  $b_2$  can also be found in Appendix B. For  $x \geq 8$ ,  $-Ei(-x)$  is set to 0. The variable  $\mathbf{x}$  is used instead of  $\frac{D_e^2}{16\delta t}$  and  $\frac{L^2}{\delta t}$  in equation 3.11.

By utilizing the equation 3.14 in section 3.3.3, the total temperature rise of the conductor and sheath was calculated.

### 5.1.4 Resulting calculation algorithm based on IEC standards

To give an overview of the order of which calculations are done in the developed algorithm, a flow chart showing how the MATLAB code in Appendix D calculates the temperature rise, is shown in figure 5.5.

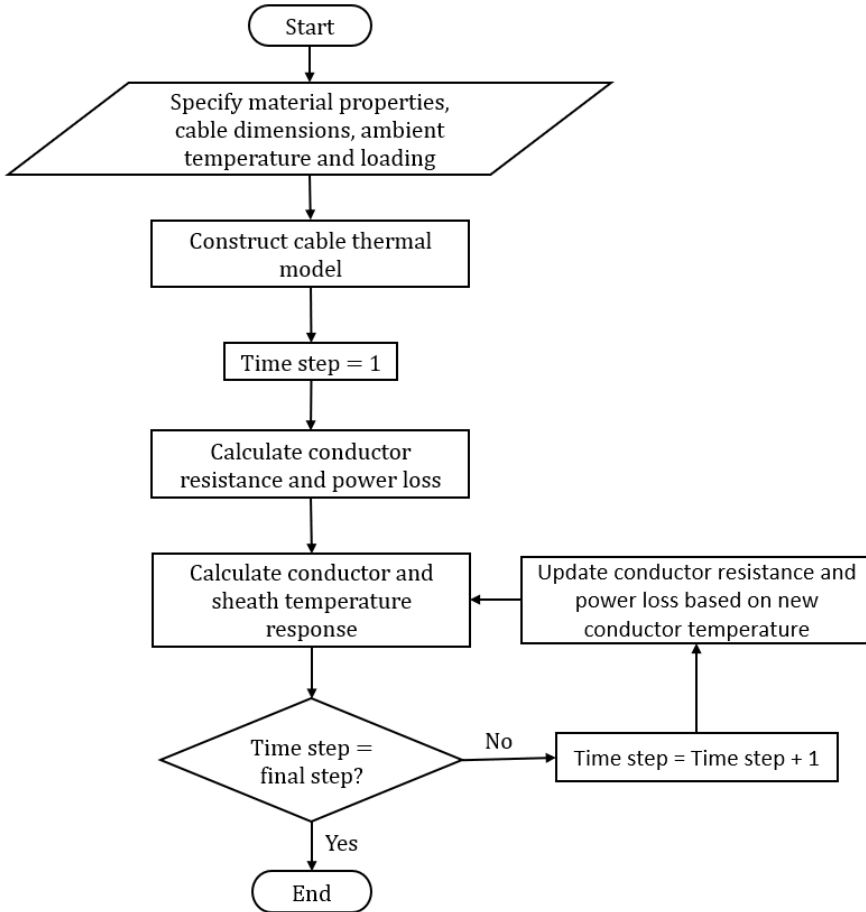


**Figure 5.5:** Flow chart of the developed algorithm for conductor and sheath temperature rise calculations based on IEC standards for cable ratings.

First, the material properties, cable dimensions, the ambient temperature and loading, are specified. Then, the transient thermal model is conducted based on the analytical modeling approach described in Chapter 3 and developed in the present chapter. Further, calculations of the conductor and sheath temperature response are performed until the specified simulation time is reached.

### 5.1.5 Temperature response of multi-step loads

The algorithm described in the previous subchapters only allow for one current step at a time. Therefore, a load profile must be divided into multiple step currents and added together by the principle of superposition (as described in section 3.3.5) in order to simulate the total temperature rise. An example on how this is done is shown in figure 5.6, where four transient temperature responses due to four current steps over a 25 hour period are added to represent the resulting temperature rise,  $\theta_{tot}$ .

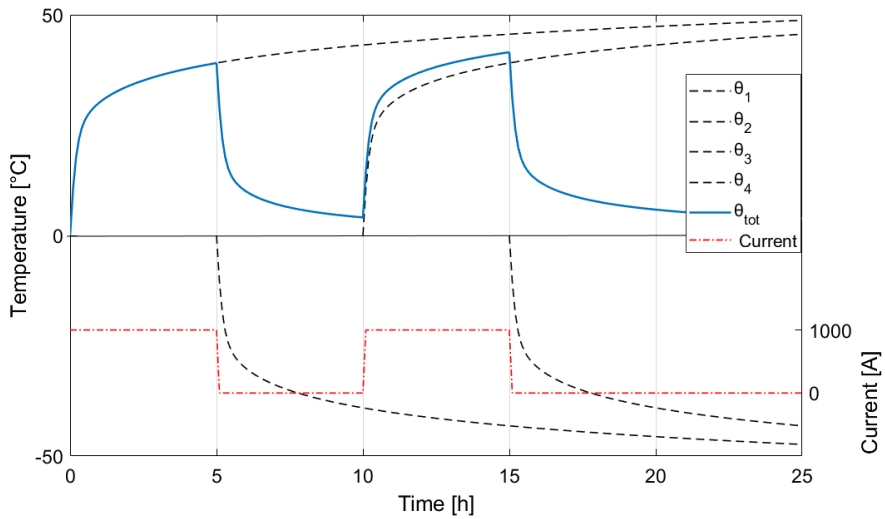


**Figure 5.6:** Total transient temperature response of multiple load steps calculated by the Superposition principle.

The figure above illustrates how the four step responses due to the four step currents result in the total temperature rise by adding them up. The step current down from 1000 A to 0 A equals a load step of -1000 A. Since the algorithm only allows for one current value at a time, the MATLAB script has to be run once for each individual current step.

## 5.2 Numerical modeling in COMSOL

This section covers the description of the numerical modeling of the cable. The model was constructed in COMSOL Multiphysics, which utilizes the finite element method (FEM) procedure. FEM simulations do not require the simplifying assumptions (*e.g.* the lumped representation) inherent in the analytical algorithms. Instead, the FEM procedure is typically based upon discretization of partial differential equations that describe physical problems. Results from the numerical model simulations were obtained to appraise the analytical approach described previously in chapter 5.1.

### 5.2.1 Model geometry

As a power cable can be assumed straight and extremely long compared to its diameter, the model was solved in the two-dimensional (2D) domain. A 2D modeling approach provides less complexity and computational effort than a full 3D simulation. Other authors ([72–76]) have proved the 2D simulation is sufficient for underground cable modeling.

#### Domain size

The outer domain, representing the soil and surrounding air was modeled as a circle, illustrated in figure 5.7. The top half of the circle represents the air, while the bottom half represents the soil. Figure 5.7 also shows the burial depth of the cable.

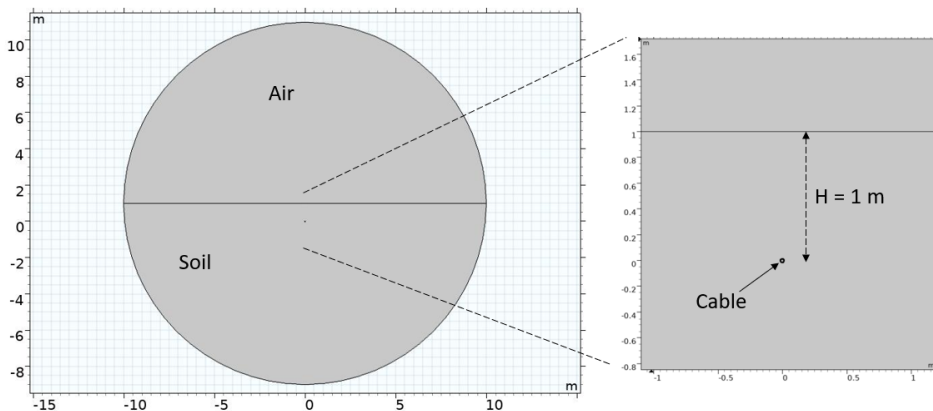


**Figure 5.7:** Total domain and burial depth of the cable of in the COMSOL model.

The needed domain size was evaluated by performing a sensitivity test on the domain radius. Steady-state conductor temperature was simulated as a function of domain size by



doing a parametric sweep of the domain radius, as shown in figure 5.8. A larger domain size will lead to more accurate simulation results, but may also make the simulation unnecessarily time consuming.

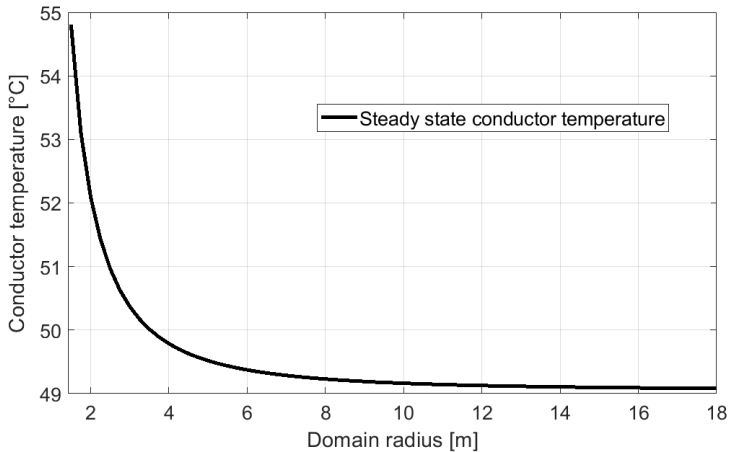


**Figure 5.8:** Steady-state conductor temperature as a function of domain size.

Furthermore, the domain size sensitivity of the model was also tested with regard to dynamic conditions. This was done by simulating a step load lasting for 500 hours, for different domain sizes, as shown in figure 5.9.

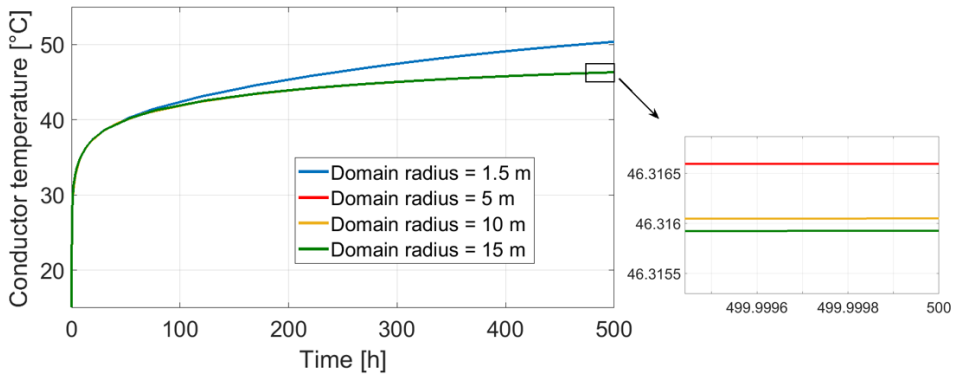


**Figure 5.9:** Conductor temperature as a function of time for different domain sizes.

From figure 5.8 and figure 5.9, a radius beyond 10 meters will not provide a significant gain in the temperature calculation accuracy. A domain radius of 10 meters was therefore chosen.

### Cable dimensions

The different cable parts (*e.g.* insulation layer) were modeled as several concentric circles. Figure 5.10 illustrates the cross section of the cable model designed according to the cable dimension data given in table 5.1.

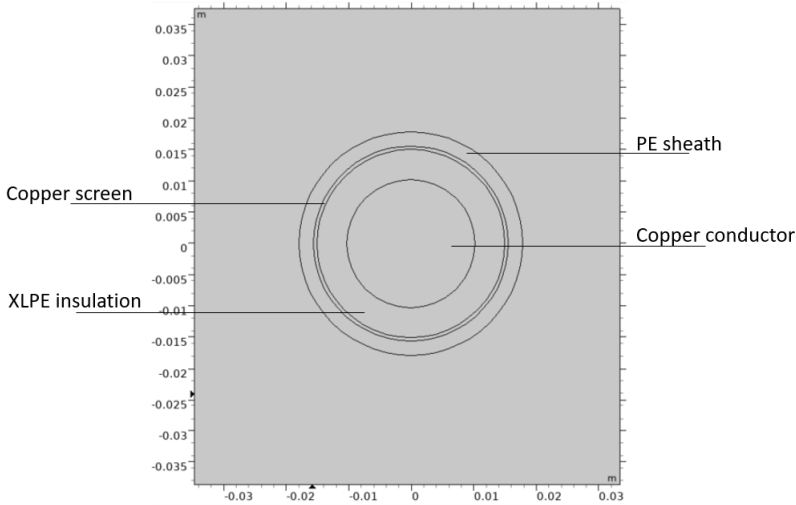


**Figure 5.10:** Cross section of the 10 kV single core cable in COMSOL.

### 5.2.2 Material properties of the cable parts and its surroundings

In the analytical approach based on the IEC standards, thermal resistivity and volumetric heat capacity had to be specified for the different materials. For the COMSOL simulations however, thermal conductivity, heat capacity at constant pressure and density for the cable materials and soil are needed.

Material properties for the XLPE insulation and PE sheath were gathered from Table 9.1 in Anders [15], while the properties for the copper conductor and screen was obtained from the Materials library in COMSOL. For the surrounding soil, the thermal conductivity was chosen as 1 K·m/W, according to the IEC standard [60], while the heat capacity and density was chosen from Steen [77]. Thermal conductivity, heat capacity and density for the for the cable materials and surrounding soil are shown in table 5.8.

**Table 5.8:** Thermal conductivity, heat capacity and density for the cable materials and surround soil used in COMSOL simulations.

	Thermal conductivity [W/K·m]	Heat capacity [J/kg·K]	Density [kg/m <sup>3</sup> ]
<b>Copper (Conductor and screen)</b>	400	385	8960
<b>XLPE/PE (Insulation and sheath)</b>	1/3.5	1850	1300
<b>Soil (Surroundings)</b>	1	1180	1600

### 5.2.3 Physics interface and solver modules

This section describes the Physics interface and the solution Study that has been used in the COMSOL simulation.

#### Heat transfer in solids

For a directly buried cable, mainly conductive heat transfer is causing the heat dissipation. To simulate the conductive heat transfer in the cable itself and its surrounding soil, the Heat Transfer in Solid physics was applied to the domain beneath the ground surface. This interface solves the following differential equation describing heat transfer by conduction [58]:

$$C_v \frac{\partial \theta}{\partial t} = \frac{\partial}{\partial x} \left( \lambda \frac{\partial \theta}{\partial x} \right) + \frac{\partial}{\partial y} \left( \lambda \frac{\partial \theta}{\partial y} \right) + W_c \quad (5.20)$$

Where:

- $C_v$  = volumetric heat capacity of the material [J/(K·m<sup>3</sup>)]
- $\theta$  = temperature [°C]
- $\lambda$  = thermal conductivity of the material [W/K·m]
- $\frac{\partial}{\partial x}$  = temperature gradient in  $x$  direction
- $\frac{\partial}{\partial y}$  = temperature gradient in  $y$  direction
- $W_c$  = heat generated in the conductor [W/m]

The heat generated in the cable was simulated by modeling the conductor as a heat source caused by the conductor loss as described previously:

$$W_c = I^2 R_\theta \quad (5.21)$$

In which  $R_\theta$  is the temperature dependent conductor resistance and  $I$  is the current.

### Time Dependent Study

To investigate the transient temperatures, the Time Dependent Study step was chosen. This study step solves the heat transfer physics in the time domain. The direct solver Pardiso was employed for the computations.

### 5.2.4 Boundary conditions

In this section, the thermal conditions needed to represent the thermal environment of the model are presented.

#### Ambient temperature

At the soil surface and the surrounding air, the isothermal boundary condition was applied, in which the temperature was held constant at 15 °C. This is indicated by the blue line in figure 5.11.

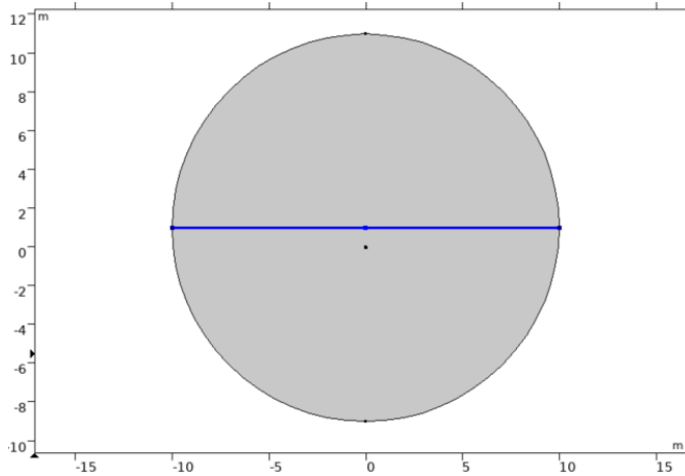


**Figure 5.11:** Isothermal boundary condition (constant temperature of 15 °C at the soil surface).

The burial depth used for underground cables will generally justify the assumption that soil surface is isothermal [51]. Moreover, the elements used in FEM calculations are small where the temperature gradients are high, which for all practical purposes justifies an assumed isothermal soil surface.

### Thermal insulation

For the soil part of the domain (lower part of the domain circle), thermal insulation was applied, as indicated by the blue line in figure 5.12. Initial conditions of the soil temperature at all depths was set to 15 °C.

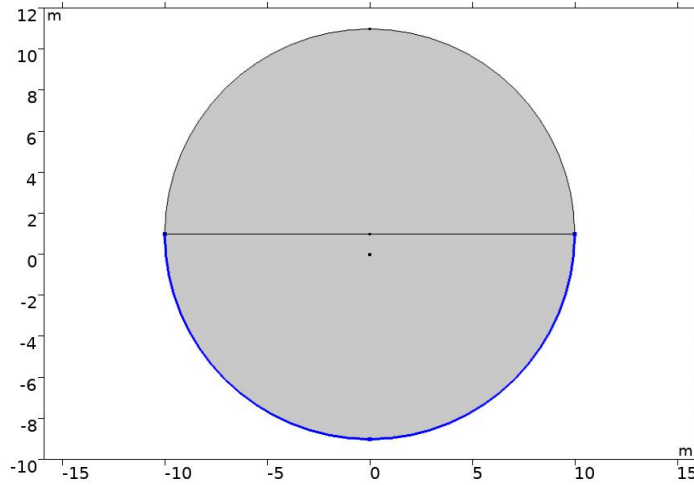


**Figure 5.12:** Thermal insulation boundary condition applied to the soil part of the domain.

By thermal insulation it is meant that there is no heat flux across that boundary. The description of this boundary condition, saying that the temperature gradient across the boundary is zero, is shown in equation 5.22. Heat cannot transfer through this boundary since there is no temperature difference [78].

$$- N \cdot q = 0 \quad (5.22)$$

In which:

- $q$  = heat flux [W/m<sup>2</sup>]
- $N$  = normal vector of the boundary surface

### 5.2.5 Meshing

Correct meshing affects the accuracy of the simulations as well as the computation time. Mesh elements should be small where temperature gradients are high and where accuracy of the calculations is important. This is typically near the cable, since interesting values are sheath and conductor temperatures. Therefore, smaller elements should be applied in and around the cable, whereas in the overall soil field, the elements can be made very large. Illustration of the mesh is shown in figure 5.13.

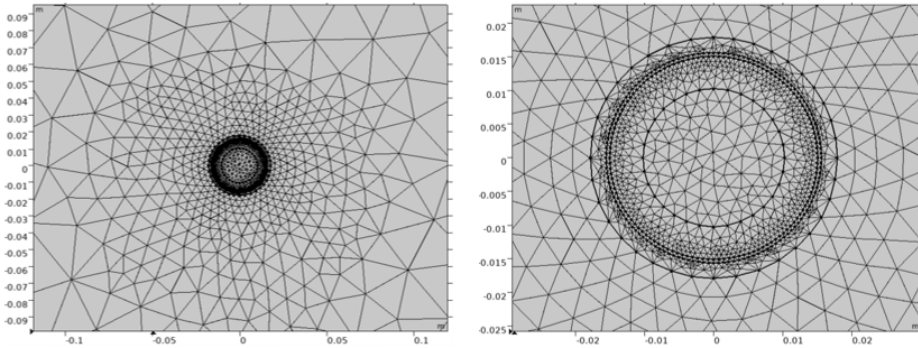


**Figure 5.13:** Illustration of the mesh for the cable and its surroundings. The mesh density is high near the cable

For the purpose of this model it was sufficient to do a Physics-Controlled Mesh with Normal Element size. Figure 5.13 shows the high mesh density in important parts of the model (*i.e.* near the cable).

## Overloading case examples

In this chapter, various overloading case examples are described. The case examples were carried out in order to investigate for how long and to what extent the cable in 5.1 may be overloaded for various scenarios. In addition, the aging of the cable insulation due to overloading was estimated.

### **6.1 Overloading capacity with various combinations of overloading current and initial load**

First, the analytical model was simulated with various combinations of overload currents and initial load prior to overloading, to evaluate the time until maximum permitted conductor temperature of 90 °C was reached. The term "overload current" is used for loads exceeding the rated current of 700 A. For example, an overload current of 60% is defined as a current 60% higher than rated current. Therefore, a 60% overload current equals to 1.6 times rated current. An "initial load" of 60% however, equals rated current times 0.6. With initial loading, it is meant average load the cable has been subjected to over a period of time until steady conditions are reached.

Time to reach maximum permitted conductor temperature of 90 °C was simulated for different combinations of overloading ranging from 60% (1120 A) to 100% (1400 A) and initial loads varying from 25% (175 A) to 100% (700 A).

Further, the maximum conductor temperature limit was increased to 100 °C and 110 °C, to investigate how higher temperature limits would affect the permitted overloading time for the same combinations of overload currents and initial load.

## 6.2 Permitted overloading for 6 hours and 24 hours

To mitigate network constraints (*e.g.* during emergency situations), it is important that the power system is able to carry loads exceeding the continuous ampacity rating for short time periods. It was therefore of interest to study the permitted overload currents for overloading situations lasting for 6 hours and 24 hours, respectively. The maximum permitted current for the 6 hours and 24 hours overloading scenario was evaluated for a 90 °C, 100 °C and 110 °C conductor temperature limit. Prior to the two overload periods an initial load of 75% (525 A) was assumed.

## 6.3 Additional aging during overload conditions

Operating temperatures during overload conditions are higher than during normal load conditions and will thus lead to a higher aging rate. It was of interest to investigate how much the overload profiles of the 6 hours and 24 hours overloading scenarios would affect the total lifetime of the cable. This is however a difficult task without performing accelerated stress tests for the given insulation type at elevated temperatures. In the literature, little is found on specific numbers for aging rates of the cable insulation as it will depend on a number of parameters, such as laying conditions and type of insulation.

However, Jensen [8] obtained some aging rates for various temperatures for XLPE insulation based on lifetime data published in Montanari and Motori [79]. These aging rates were used to give an indication on how the cable lifetime would be affected by the given overload scenarios. The aging rates for different operating temperatures are recalled in table 6.1.

**Table 6.1:** Aging rates for various operating temperatures for XLPE insulation, based on lifetime data in Montanari and Motori [79].

Temperature [°C]	Lifetime [h]	Aging rate [% h <sup>-1</sup> ]
140	300*	0.345634828
135	500*	0.219294289
130	1 000*	0.137573881
120	2 000*	0.052251873
110	5 000*	0.018867813
100	9 000*	0.011111111
90	48 098**	0.002079076
80	159 125**	0.000628435
60	2 160 436**	0.000046287
40	40 929 899**	0.000000247
30	1 158 386 103**	0.000000086

\*Given from accelerated stress test in [79].

\*\*Estimated in [8] based on the Arrhenius model.



Based on the values in table 6.1, an exponential function was derived to represent the aging rates of an XLPE insulated cable as a function of temperature. The function was plotted in logarithmic scale to display how the aging rate of XLPE changes with temperature, as shown in figure 6.1.

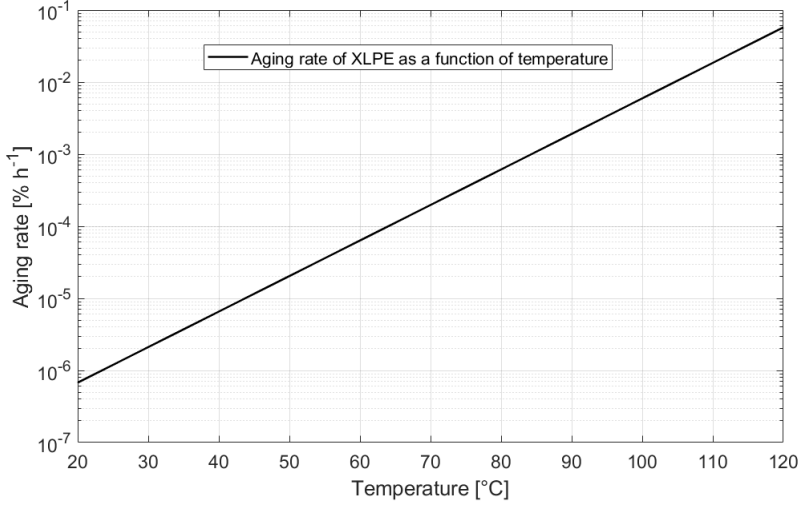


**Figure 6.1:** Aging rate for an XLPE insulated cable based on lifetime data published in [79] and [8].

To calculate the total thermal lifetime consumption during overload conditions, the total loss of life (aging) factor caused by the given overload profile, was calculated from equation 6.1, as described in section 4.2.

$$L_f = \sum_{i=1}^K R_{a,i}(\theta) \cdot t_{D,i} \quad (6.1)$$

Where  $R_{a,i}(\theta)$  is the aging rate for the specific temperature at the  $i^{th}$  interval and  $t_{D,i}$  is the time period of which the aging rate is acting. Based on the lifetime vs. temperature relationship for XLPE cables carried out in Shwehdi et al. [7], the total cable lifetime was set to 40 years, which is considered reasonable for an XLPE power cable. To calculate the total lifetime consumption in percentage of the total lifetime, the total loss of life from equation 6.1 was multiplied with the assumed total lifetime of 40 years.

At low temperatures, the influence of thermal aging is negligible. From table 6.1 it can be seen that estimated lifetime at temperatures from 60 °C and below are so long that the additional thermal aging from these temperatures can be neglected when calculating the lifetime consumption from the overload profiles. The estimated lifetime at constant operating temperature of 60 °C is 2 160 436 hours (~250 years), which is way beyond the assumed lifetime of 40 years. Therefore, only aging rates for temperatures exceeding

this threshold of 60 °C were used in the calculation of total lifetime consumption by the 6 hours and 24 hours overload profiles.

To explain the aging calculation method in detail, a simplified conductor temperature profile in figure 6.2 is utilized to calculate extra aging due to temperatures exceeding the threshold of 60 °C.

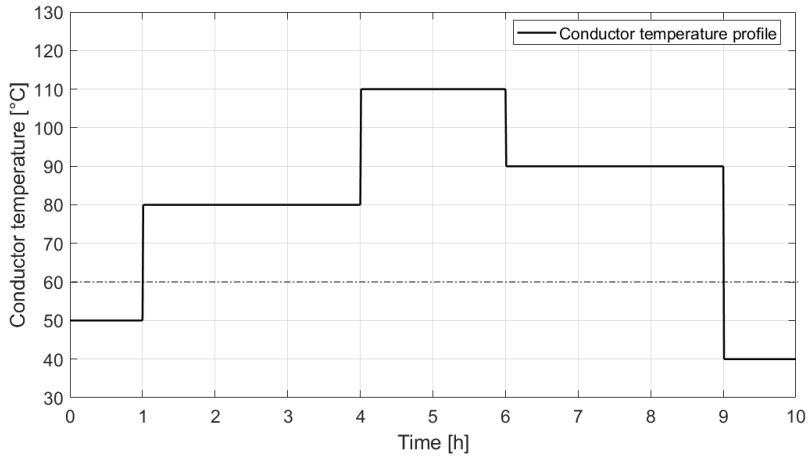


**Figure 6.2:** Conductor temperature in a simplified case.

For time intervals where conductor temperature is 60 °C or above, the corresponding aging rate is used to calculate the loss of life factor due to the specific temperature during that time period. To compute the total aging, the loss of life factor for the given time period at that specific temperature is multiplied with the assumed total lifetime of the cable. Table 6.2 shows the total lifetime consumption of the simplified temperature profile in figure 6.2.

**Table 6.2:** Total lifetime consumption (aging) of the cable lifetime due to the temperature profile in figure 6.2.

Time period [h]	Temperature [°C]	Aging rate [% h <sup>-1</sup> ]	Aging [% of lifetime]	Aging [h]
0 - 1	30	0	0	0
1 - 4	80	0.000628435	0.0018853	6.6
4 - 6	90	0.002079076	0.0041582	14.6
6 - 9	110	0.018867813	0.0566034	198.3
9 - 10	40	0	0	0
<b>Total aging [h]</b>				<b>219.5</b>

## Results and discussion

In this chapter, the obtained results from the transient thermal cable modeling are presented and discussed. First, a comparison of the analytical approach based on the IEC standards and the numerical model constructed in COMSOL, is given. Further, the analytical approach is tested on a cyclic load profile to show how the principle of superposition may be utilized to calculate total temperature rise due to a multi-step load profile.

Further, the results from the different combinations of overload currents and initial load prior to overloading, are presented and discussed. It is also evaluated how interpretation of sheath temperature measurements can be utilized for estimating the conductor temperature.

Furthermore, the permitted overloading for 6 hours and 24 hours is calculated for the various conductor temperature limits. Moreover, the estimation of additional aging due to elevated temperatures during overloading, is presented.

Lastly, an evaluation on how air ambient temperature variations will affect the soil temperature at burial depth is given. It is also shown how seasonal temperature variations of the soil will affect the conductor temperature calculations and thus rating of the cable.

## 7.1 Comparison of the analytical and numerical modeling approach

An analytical algorithm to calculate both the conductor temperature and sheath temperature was compiled on the basis of the conventional IEC standards for rating of power cables. A numerical model was established in COMSOL for comparison of the developed analytical model. The purpose of this comparison was to appraise the suggested method for transient temperature calculations based on the IEC standards.

First in this section, calculations of transient sheath and conductor temperatures from the analytical and numerical model are compared by applying a step current from no-load conditions. Further, the two models are also compared by applying a full-load-to-no-load step current. Lastly, the results from the two comparison tests are discussed.

### 7.1.1 Step response of a step current from a no-load condition

The first comparison of the two modeling approaches was performed with a step current of full load (700 A). Prior to the current step, the cable was unenergized, *i.e.*, both the conductor and sheath were at an ambient temperature of 15 °C. Figure 7.1 shows the conductor and sheath temperature for the first 1000 hours, calculated in COMSOL and by the analytical algorithm based on IEC standards.

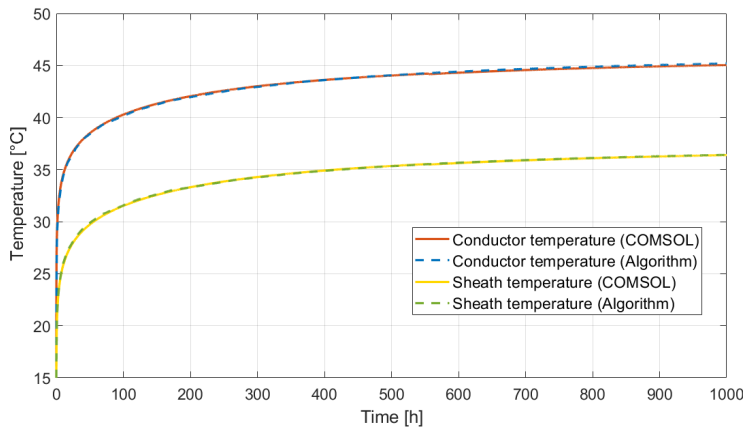


**Figure 7.1:** Transient temperature response for a full-load step current (700 A) applied for 1000 hours, to compare the analytical algorithm with the COMSOL model. Prior to the current step, the cable was unenergized, *i.e.*, both the conductor and sheath were at an ambient temperature of 15 °C.

From figure 7.1 it can be seen that the transient temperature calculations, both for sheath temperature and conductor temperature, were more or less similar for the analytical algorithm and the COMSOL model. However, it is difficult from figure 7.1 to draw concrete conclusions on the exact deviation between the two modeling approaches. Therefore, the temperature deviation of the numerical and analytical modeling was plotted, which is shown in figure 7.2.

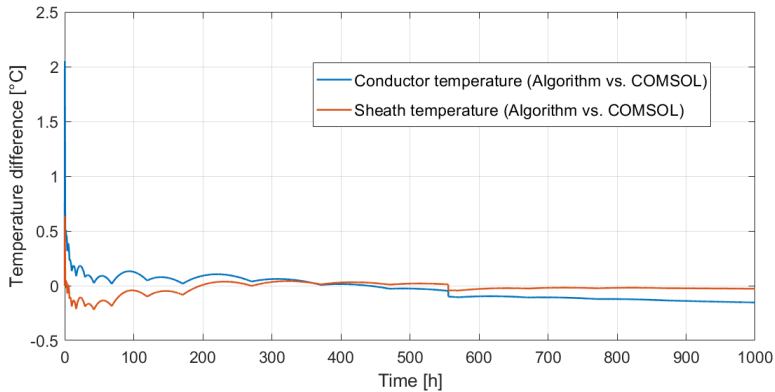


**Figure 7.2:** Deviation between the analytical algorithm and the COMSOL model for conductor and sheath temperature calculations. A full-load step current (700 A) is applied for 1000 hours.

It can be observed from figure 7.2 that the largest deviation in calculated conductor temperature from the analytical model and the COMSOL model, is just over 2 °C. For the sheath temperature however, the largest deviation is approximately 0.6 °C. The largest deviation between the two calculation approaches occurs close to 30 minutes after the step current is applied.

### 7.1.2 Step response of a full-load-to-no-load step current from a no-load condition

In the second comparison scenario, a full-load-to-no-load current step was applied to investigate how well the analytical algorithm matches the COMSOL model when utilizing the superposition principle. Initial temperature conditions prior to the current step are at ambient temperature, as the cable is unenergized prior to the step load. Figure 7.3 shows how the conductor and sheath temperature varies with the load applied. A step load of rated current is applied for 50 hours, followed by a no-load condition for another 50 hours.

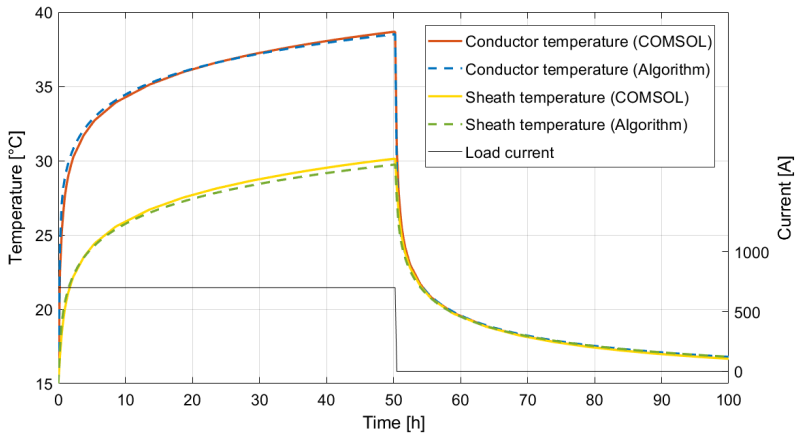


**Figure 7.3:** Transient temperature response to compare the analytical algorithm with the COMSOL model. A full-load step current (rated current) is applied for 50 hours, followed by a no-load condition for another 50 hours.

Figure 7.3 shows that there is little deviation between the temperatures computed from the analytical approach and the COMSOL model for a full-load-to-no-load step current. This verifies that the superposition principle works for calculating total temperature rise from a load profile consisting of more than one step current. As the cable cools down after being at rated current for 50 hours, both the conductor temperature and sheath temperature move towards the ambient temperature of 15 °C. Figure 7.4 shows the deviation between the two modeling approaches through the whole load period, for both sheath and conductor temperature.

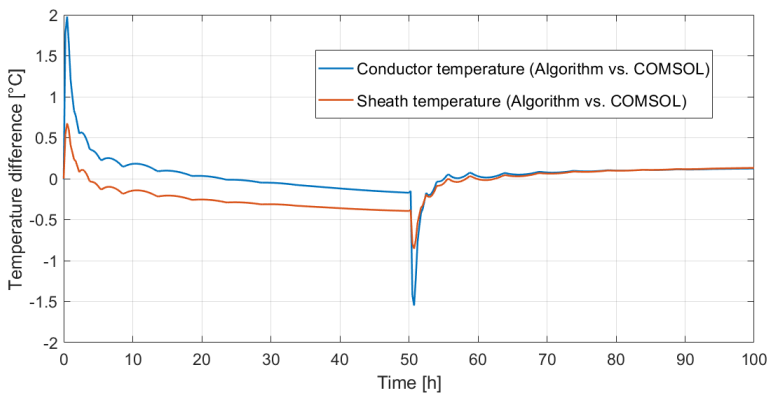


**Figure 7.4:** Deviation between the analytical algorithm and the COMSOL model for conductor and sheath temperature calculations. A full-load step current (rated current) is applied for 50 hours, followed by a no-load condition for another 50 hours.

From figure 7.4, it can be seen that the largest deviation between the two modeling approaches occurs approximately 30 minutes after a change in applied current (both for a step up current and a step down current). When unenergizing the cable after it has been at full-load for 50 hours, the largest deviation is approximately 0.8 °C and 1.5 °C for the sheath temperature and conductor temperature, respectively.

### 7.1.3 Discussion on the comparison of the analytical and numerical modeling approach

Results from the comparison of the analytical and numerical modeling showed little deviation of the transient temperature calculations, both for the conductor and sheath temperature. When two generic different models calculate the same temperatures, it is likely that the modeling is correct. However, this does not exclude the usage of erroneous or inaccurate material data.

For the cable parts, the material properties are equal for both models. However, the analytical approach only takes thermal resistivity and diffusivity into account for the surrounding soil, whereas COMSOL models the soil with values for thermal conductivity (reciprocal thermal resistivity), density and heat capacity.

The diffusivity of the soil was, as an initial approximation, set to  $5 \cdot 10^{-7} \text{m}^2/\text{s}$  in the analytical approach. By utilizing the same soil property data as used in the COMSOL model, the diffusivity could have been calculated from equation 3.13. From the data set for soil property in table 5.8 and equation 3.13, the correct value for diffusivity would have been  $5.3 \cdot 10^{-7} \text{m}^2/\text{s}$  (6% higher than the chosen value of  $5 \cdot 10^{-7} \text{m}^2/\text{s}$ ).

To investigate how much this erroneous approximation of the diffusivity coefficient has affected the results, the analytical model was simulated with three different values of diffusivity over a time period of 1000 hours. The cable was unenergized prior to the current step and applied rated current at  $t = 0$ . The conductor temperature step response for the three different diffusivity values are shown in figure 7.5.

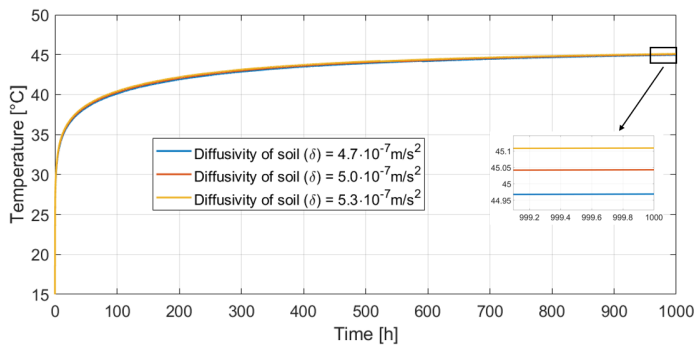
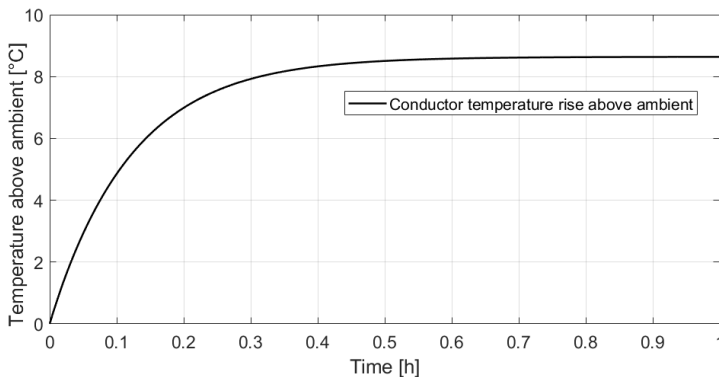


Figure 7.5: Conductor temperature response with three different values of soil diffusivity.

As figure 7.5 shows, the slightly inaccurate value of chosen diffusivity did not cause a noteworthy change in calculated temperature after 1000 hours. A change in diffusivity of  $\pm 6\%$  resulted in a deviation in calculated conductor temperature of approximately  $\pm 0.16\%$ , which is more or less negligible. Therefore, for all practical purposes, the approximated value used for diffusivity in the analytical model is not likely to have had any significant impact on the obtained results.

Moreover, the transient temperature rise in figure 7.1 consists of a fast component caused by the rapid heating of the internal parts of the cable, and a slow component which describes the slow heating of the soil. It can be seen from figure 7.2 and figure 7.4, that the biggest deviation between the two models were found shortly after a change in the applied load.

Shortly after a change in applied load, it is only the heating of the internal cable parts that will affect the total temperature rise of the cable. The fast heating of the conductor is an adiabatic process where no heat is transferred to the surroundings. Thermal properties of the soil will therefore not affect the temperature rise in this transient period. The fast component caused by the rapid heating of the internal parts of the cable, determined from the analytical modeling approach, is depicted in figure 7.6.

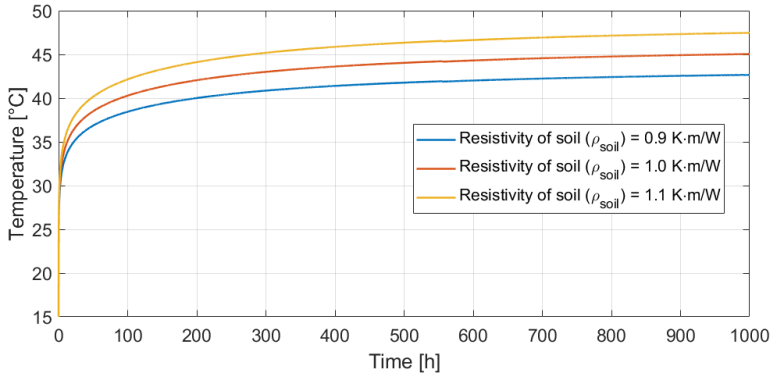


**Figure 7.6:** Conductor temperature rise above ambient for the first hour after applying a step load of rated current.

Figure 7.6 shows that the cable conductor will reach its final temperature rise above ambient 30 minutes after a load step of rated current is applied. This is the same point (time) as when the largest deviation between the two modeling approaches occurs from figure 7.2 and figure 7.4. The conductor temperature rise above ambient calculated from equation 5.10 consists of two exponential functions with time constants calculated from the transfer function. Values of these time constants describe the rate of which the conductor temperature is changing, and may be the reason for the deviation of calculated temperatures in the transient period after a change in applied current.



For buried cable systems, accurate data about the soil properties may be difficult to obtain or predict. Therefore, there will always be some insecurity as to the results of temperature calculations. For both modeling approaches, the thermal resistivity was chosen as 1 K·m/W as according to the IEC standards. In reality, the thermal resistivity of the soil may vary quite a lot both in time and location. To show how variations in thermal resistivity of the soil will affect the calculated temperatures, three different values of the thermal resistivity were simulated. Figure 7.7 shows the calculated transient temperatures when applied rated current for 1000 hours.



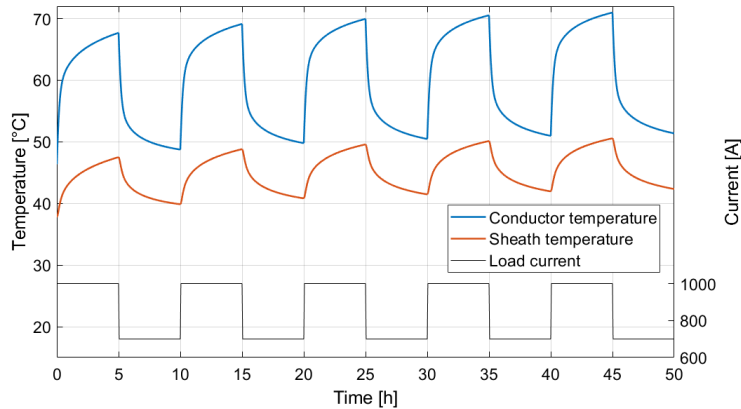
**Figure 7.7:** Transient temperature calculations with various thermal resistivity of soil.

Figure 7.7 shows a relatively big deviation in computed conductor temperature with varying soil resistivity. A change in thermal resistivity of  $\pm 10\%$  results in a deviation in calculated temperature after 1000 hours of approximately  $\pm 5.3\%$  (2.4 °C). This indicates that choosing correct values of soil properties is important for accurate temperature calculations. It also shows that appropriate values of crucial parameters are more important than the type of modeling approach that is used (analytical or numerical).

The transient temperature calculations of the analytical and numerical model are in good accordance with findings of other authors ([8, 51]) and the obtained results are hence deemed to be realistic. It would have been preferable to have measured temperature data to which the temperature calculations from both modeling approaches could have been compared to, in order to validate the results. Such data has however not been available.

## 7.2 Transient temperatures under variable loading

Figure 7.8 shows the conductor and sheath temperature calculated by the analytical approach when a cyclic load of 700 - 1000 A is applied for 50 hours. Prior to the first 1000 A step at  $t = 0$ , the cable has been at rated current (700 A) for a long period of time so that steady-state conditions are obtained.



**Figure 7.8:** Conductor and sheath temperatures when applied a cyclic load current.

In the previous section, the accuracy of using the principle of superposition was verified by comparing transient temperature calculations of the analytical and numerical model when a full-load-to-no-load current was applied. Figure 7.8 shows how the principle of superposition can be used to calculate the total temperature rise due to a cyclic load profile by dividing the current into multiple step loads.

However, the analytical algorithm only allows for one current step at a time. Which means that to obtain the total temperature rise of a load profile consisting of multiple steps, the temperature rise of each individual current has to be calculated and then added up manually. Since the temperature rise from a current step is dependent on the load history and rise of temperature at the point of which the current step is initiated, it is a rather complex process to do manually. Therefore, this process could preferably be developed to a more automatic procedure.

### 7.3 Overload conditions with varying load history prior to overloading

To investigate for how long and to what extent the cable could be overloaded with currents exceeding its rating, without violating the maximum conductor temperature limit, different combinations of overload currents and initial load prior to overloading, were simulated.

First in this section, time to reach maximum permitted conductor temperature ( $\theta_c^{max}$ ) of 90 °C and sheath temperatures at  $\theta_c^{max}$  for all combinations of overloading currents and initial loading, is presented. The values are obtained by applying overload currents ranging from 60% - 100% above rated current and initial loading conditions ranging from 25% - 100% of rated current. An example, showing transient temperature calculations for various

overload currents with an initial load of 75% of rated current, can be found in Appendix C.

Further, transient conductor and sheath temperatures are compared to investigate how information about sheath temperatures (which may be obtained by temperature measuring equipment, such as DTS), can be utilized to predict operating conductor temperature.

Lastly, the impact of increasing maximum allowed conductor temperature to 100 and 110 °C has on the permitted overloading time period, is presented.

### 7.3.1 Time to reach maximum permitted conductor temperature

Time to reach maximum permitted conductor temperature for different combinations is showed in table 7.1. The corresponding sheath temperatures at maximum permitted conductor temperature, for the different combinations of initial load and overloading, can also be seen from the table. The time to reach maximum permitted conductor temperature is rounded up to the closest integer.

**Table 7.1:** Time to reach maximum permitted conductor temperature ( $\theta_c^{max}$ ) and sheath temperature at  $\theta_c^{max}$  for different combinations of initial loading and overloading.

		Overload					
		60% (1120 A)	70% (1190 A)	80% (1260 A)	90% (1330 A)	100% (1400 A)	
Initial load prior to overloading	25% (175 A)	Time to reach $\theta_c^{max}$ * Sheath temp. at $\theta_c^{max}$	80 hours 61.2 °C	24 hours 56.0 °C	9 hours 50.8 °C	4 hours 45.0 °C	2 hours 41.2 °C
	50% (350 A)	Time to reach $\theta_c^{max}$ Sheath temp. at $\theta_c^{max}$	70 hours 61.2 °C	20 hours 56.1 °C	7 hours 51.2 °C	3 hours 46.4 °C	2 hours 42.2 °C
	75% (525 A)	Time to reach $\theta_c^{max}$ Sheath temp. at $\theta_c^{max}$	54 hours 61.2 °C	14 hours 56.5 °C	5 hours 51.9 °C	2 hours 47.9 °C	1 hour 43.8 °C
	100% (700 A)	Time to reach $\theta_c^{max}$ Sheath temp. at $\theta_c^{max}$	30 hours 61.6 °C	7 hours 57.3 °C	2 hours 53.7 °C	1 hour 50.6 °C	<1 hour 47.4 °C

\* $\theta_c^{max}$ : Maximum allowed conductor temperature (typically 90 °C for XLPE cables)

From table 7.1, it can be seen that in case of an initial load of rated current (100%) and a temperature limit of 90 °C, an overload current of 60% (a current 60% higher than rated current), can be applied for 30 hours. The results show that time to reach 90 °C is not only dependent on the overload current that is applied, but also on the average loading that has been applied prior to overloading. In the case of an 60% overload current, the cable can be overloaded for 50 hours more if initial loading conditions are at 25% instead of 100% of rated current. Therefore, knowledge about loading history, is a very important factor for utilities when they are deciding for how long and to what extent the cable may be overloaded.

For high overloading (say 80% over rated current and above), the permitted overloading time is under ten hours for all initial loading conditions. For 100% overloading,  $\theta_c^{max}$  is reached within two hours independent of the initial loading. The time required to reach maximum conductor temperature decreases significantly as the overload current increases, for all initial load scenarios. This is due to the fact that conductor losses are proportional to the current squared.

In the case of a 60% overload current, the measurable sheath temperatures at maximum permitted conductor temperature,  $\theta_c^{max}$ , are similar (around 61 °C in this case), independent of the initial loading. This is also the case for the 70% overload case, where measurable sheath temperature only deviates with 1.3 °C from an initial condition of 25% versus 100% of rated current. This indicates that when overloading is permitted for long time durations, the initial load prior to overloading will not affect the measurable sheath temperature.

At high overloading (say 80% over rated current and above), there is a relatively big deviation between the sheath temperatures at  $\theta_c^{max}$ , depending on the initial loading. The measurable sheath temperature at  $\theta_c^{max}$  for the combination of 25% initial load and 100% overloading is 41.2 °C, whereas the sheath temperature is 47.4 °C at  $\theta_c^{max}$  for the combination of 100% initial load and 100% overloading. The deviation in measurable sheath temperature at the same conductor temperature ( $\theta_c^{max}$ ) for high overloading, indicates that the sheath temperature is changing in a different manner than the conductor temperature. This is looked more into in the next subchapter.

### 7.3.2 Conductor temperature vs. measurable sheath temperature

As it was shown in figure 7.6 from section 7.1.3, the conductor temperature rise above ambient changes immediately after a current step is applied. The sheath temperature will however, due to thermal mass of the cable, heat in a slower manner.

Figure 7.9 shows how the conductor temperature and sheath temperature change the first half an hour of a 60% overload current. Prior to the overloading, it is assumed that the average cable loading has been at 75% for a sufficient period of time to reach steady-state conditions, while the overload current is applied at time  $t = 0$ .

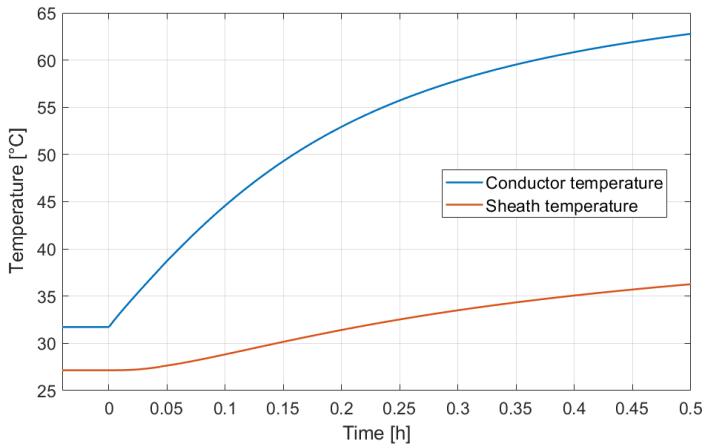


**Figure 7.9:** Transient conductor and sheath temperature the first half hour after applied an overload step current. Prior to the overload current, the average load is assumed to be 75% of rated current.

It is clear from figure 7.9 that the conductor temperature will rise immediately after a step-current is applied. For the sheath temperature however, the temperature is changing in a slower manner. For the first couple of minutes after the current step, there is no change in the measurable sheath temperature. This indicates that when monitoring sheath temperature with measuring equipment (such as DTS systems), not only the absolute temperature should be measured. It is also of interest to measure how the sheath temperature is changing with time, as this may indicate how the conductor temperature is changing.

To investigate in detail how the conductor and sheath temperature is developing over time after a step-current is applied, the time derivative of the temperature was plotted against time, as shown in figure 7.10.

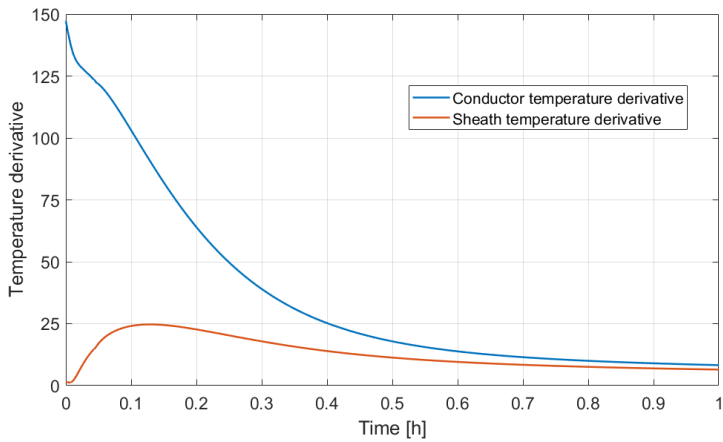


**Figure 7.10:** Time derivative of conductor and sheath temperature for the first hour of overloading at 60%, showing the rate of which the temperatures are changing.

Figure 7.10 shows that the conductor temperature changes immediately after the overload current is applied. However, the conductor temperature change decreases rather quickly and will eventually approach zero as the thermal equilibrium is reached at steady-state conditions.

For the sheath temperature however, the temperature derivative is different. The first minutes after applying a step current, there is little or no change in the measurable sheath temperature. After a couple of minutes, the temperature change increases and reaches its maximum approximately ten minutes after the current step is applied. From that point, the change in temperature decreases until thermal equilibrium is reached, as for the conductor temperature. It can also be observed that one hour after applying the step current, the change in conductor temperature and change in sheath temperature, is almost identical.

Measurements of the rate of change in sheath temperature may thus give an indication on how the conductor temperature is changing. However, at the earliest stages of the transient, the sheath temperature is changing slowly while the rate of change in conductor temperature is high. While further in the transient, both sheath temperature and conductor temperature are changing relatively slowly and at the same rate. Measurements of the rate of change in sheath temperature after, say the first hour of the transient, will give a good estimate of the rate of change in conductor temperature.

### 7.3.3 Effect of increasing the maximum conductor temperature limit

By allowing the conductor temperature to exceed its permitted limit of 90 °C, the overloading time can be extended. Therefore, it was of interest to see for how long the cable may be overloaded if maximum conductor temperature was increased to 100 °C and 110 °C, respectively. The results for different combinations of initial load and overloading are presented in table 7.2. Time to reach the temperature limits are rounded to the closest time integer. All times exceeding 100 hours are rounded to the closest day integer.

**Table 7.2:** Time to reach 100 °C and 110 °C conductor temperature for different combinations of initial load and overloading.

		Overload					
		60% (1120 A)	70% (1190 A)	80% (1260 A)	90% (1330 A)	100% (1400 A)	
Initial load prior to overloading	25% (175 A)	Time to reach 100 °C conductor temp. Time to reach 110 °C conductor temp.	10 days 46 days	61 hours 6 days	20 hours 44 hours	8 hours 16 hours	4 hours 7 hours
	50% (350 A)	Time to reach 100 °C conductor temp. Time to reach 110 °C conductor temp.	9 days 44 days	54 hours 6 days	17 hours 40 hours	7 hours 14 hours	3 hours 6 hours
	75% (525 A)	Time to reach 100 °C conductor temp. Time to reach 110 °C conductor temp.	8 days 40 days	43 hours 5 days	13 hours 32 hours	5 hours 11 hours	2 hours 4 hours
	100% (700 A)	Time to reach 100 °C conductor temp. Time to reach 110 °C conductor temp.	6 days 33 days	26 hours 86 hours	7 hours 21 hours	3 hours 7 hours	1 hour 3 hours

In the case of an overload current of 60%, table 7.2 shows that the time it takes to reach 100 °C and 110 °C conductor temperature, is in the order of days and weeks, respectively. By comparing the time to reach 90 °C from table 7.1 and time to reach 100 °C and 110 °C from table 7.2, it is clear that for most combinations of initial load and overloading, the time to reach critical temperature will generally manifold.

## 7.4 Overload case example - 6 hours and 24 hours overloading

First in this section, the permitted overload currents to reach the different conductor temperature limits is calculated, both for the 6 hour and 24 hour overloading case scenario. Furthermore, an evaluation of the additional aging the permitted overload profiles inflict on the XLPE insulation is presented.

### 7.4.1 Permitted overloading profiles based on temperature limits

To evaluate to what extent the cable could be overloaded for 6 hours and 24 hours, overload currents ranging from 40% - 100% above rated current, were applied. The conductor temperature limits were set to 90 °C, 100 °C and 110 °C. Obtained conductor temperature after 6 hours and 24 hours with the various overload currents is depicted in figure 7.11. Initial loading prior to the overloading scenarios was assumed to be 75% of rated current.

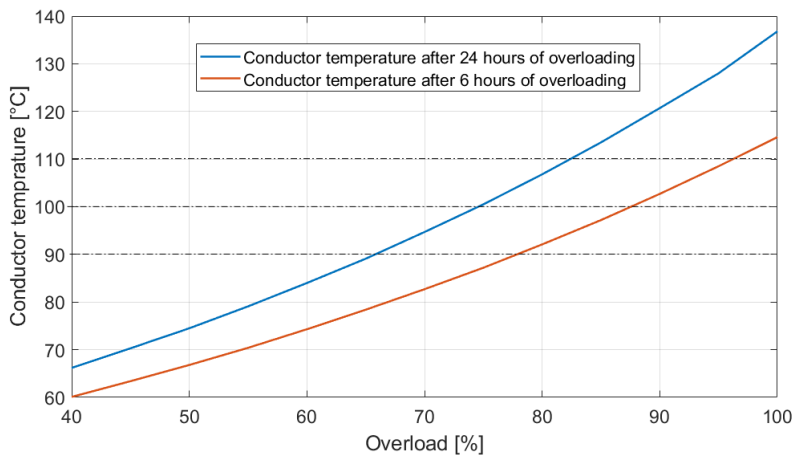


**Figure 7.11:** Permitted overload current for a period of 6 hours and 24 hours with maximum conductor temperature limits of 90 °C, 100 °C and 110 °C.

Figure 7.11 shows that if overloading is permitted for 6 hours, the maximum overload current is 78%, 87% and 96% above rated current for a 90 °C, 100 °C and 110 °C conductor temperature limit, respectively. By allowing overloading for 24 hours however, the maximum allowed overload current is 66%, 75% and 83% for the 90 °C, 100 °C and 110 °C conductor temperature limits, respectively.

Steady-state ratings for power cables are important for the overall planning of a cable



system, but by permitting cables to carry more current for short periods of time, constraints can be mitigated. For instance, if the cable circuit is connected to intermittent peak load generation.

Short-term ratings may also be valuable if a fault in neighbouring circuits occurs. For example, consider two equal cable circuits as the one modeled in this report, in which there is a fault in one of them. If the reparation time of the faulted cable is less than 6 hours, almost all the power may be transmitted through the non-faulted cable, if maximum permitted conductor temperature is set to 110 °C. This is however for a cable loaded at 75% of the rated current prior to the fault. The available 6 hour overload capacity would be lower for a higher pre-fault current and higher if the pre-fault cover was lower than 75%.

Figure 7.12 shows the conductor temperature after 6 hours, when applying overload currents of 78%, 87% and 96% above rated current, for different values of initial loading.

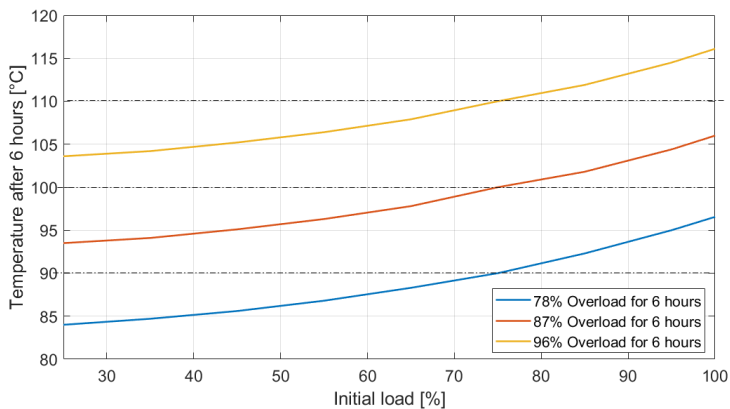


**Figure 7.12:** Conductor temperature after 6 hours of overloading at 78, 87 and 96% above rated current as a function of initial load.

Figure 7.12 shows that initial loading prior to the 6 hour overloading case will affect the resulting conductor temperature. The conductor temperature after an overload current of 78% is applied for 6 hours, is 5 °C lower if initial load prior to overloading is assumed to be 40% instead to 75%.

### 7.4.2 Thermal aging due to overloading profiles

Figure 7.13 shows the permitted overload profiles, based on maximum permitted conductor temperature of 90 °C, 100 °C and 110 °C, for the 6 hours and 24 hours overloading cases. Initial load prior to overloading is 75% of rated current.

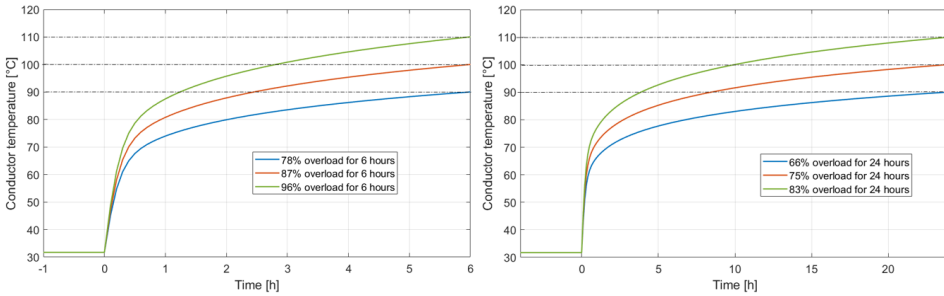


**Figure 7.13:** Overloading profiles of 6 hours and 24 hours for maximum temperature of 90 °C, 100 °C and 110 °C. Initial load prior to overloading is 75% of rated current.

The increased temperature due to overloading will cause additional aging of the insulation material as a result of increased chemical reaction rates. By utilizing the aging rates and calculation method outlined in section 6.3, the total lifetime consumption caused by the various overloading profiles was estimated, as shown in table 7.3.

**Table 7.3:** Total aging due to overload profiles in figure 7.13.

Overload profile	Max. conductor temp. [°C]	Total aging [h]	Total aging [% of lifetime]
78% overload for 6 hours	90	20	0.0057
87% overload for 6 hours	100	56	0.0160
96% overload for 6 hours	110	159	0.0453
66% overload for 24 hours	90	85	0.0243
75% overload for 24 hours	100	241	0.0688
83% overload for 24 hours	110	683	0.1949

Table 7.3 shows that in the case of a conductor temperature limit of 90 °C, the permitted overloading currents for the 6 hours and 24 hours cases, will caused additional aging of 20 hours and 85 hours, respectively. When assuming that total lifetime of the cable is 40 years (350 400 hours), a total lifetime consumption of 20 hours and 85 hours is less negligible. The 78% overload profile lasting for 6 hours, can be applied 175 times (more than four times a year over 40 years), without causing additional aging that would consume more than 1% of the cable total lifetime.

In the case of an overload current of 83% applied for 24 hours, the cable lifetime was reduced by approximately one month. This is only 0.2% of the total expected cable lifetime of 40 years.

Table 7.3 also shows that by increasing the temperature limit with 10 °C (from 90 °C to 100 °C), the total lifetime consumption approximately triples. By increasing the temperature limit to 110 °C, the lifetime consumption will be eight times higher than for a 90 °C temperature limit.

As the operating temperature increases due to overloading, it is shown that expected lifetime of the cable will slightly decrease. Therefore, utilities must consider whether this additional operational flexibility of the cable system is worth consuming some of the cable lifetime. However, the aging calculated in this section is only due to thermal degradation. Other aging mechanisms will also impact on the insulation lifetime, but they are not looked into in this thesis.

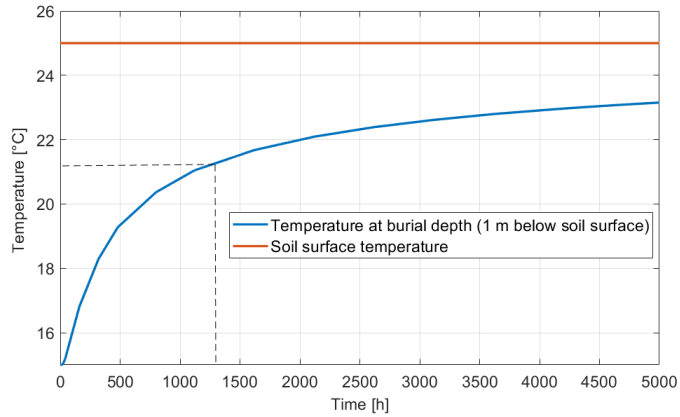
## **7.5 Temperature variations in the soil**

Up until now, all simulations have been performed with a constant ambient temperature of 15 °C. However, air ambient temperature will vary significantly, thus the soil temperature at burial depth will also change. First, a sensitivity analysis reaffirming whether varying air temperature is likely to cause changes in temperature at burial depth during a transient, is presented. Further, the impact seasonal temperature variations have on the cable rating was investigated.

### **7.5.1 Air ambient temperature influence on soil temperature**

Air ambient temperature is a measurable parameter that may be utilized when rating power cables. However, for underground cables, the impact of changes in weather conditions is slow and complicated. Therefore, a change in the air ambient temperature may not affect the transient rating of such cable systems. To investigate this, a sensitivity analysis on how a step increase in air ambient temperature affects the soil temperature at burial depth, was performed.

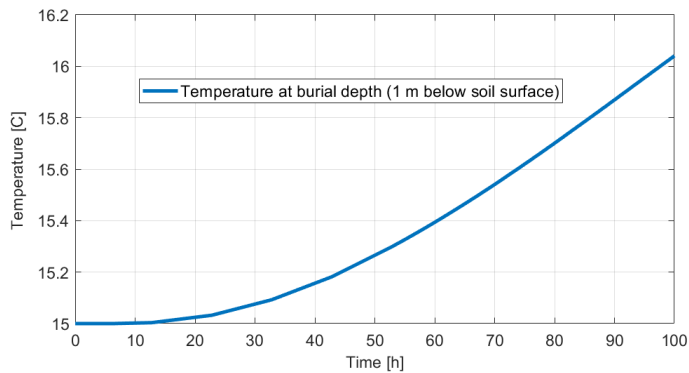
The COMSOL model described in chapter 5.2, was run with a step change in air temperature of 10 °C (from 15 °C to 25 °C). The cable was unenergized during this sequence. The temperature at burial depth (1 meter below the soil surface), was simulated to show the time it takes to change the temperature at this depth with a change in air ambient temperature. Figure 7.14 shows the temperature development at burial depth for the first 5000 hours.



**Figure 7.14:** Soil surface temperature and temperature development at burial depth for a step increase in air ambient temperature of 10 °C (from 15 °C to 25 °C) for 5000 hours.

Figure 7.14 shows that the thermal time constant at burial depth is around 1300 hours. The long time constant indicates that the temperature at burial depth will not be affected by an increase in air ambient temperature for transients overloading periods. This is a crude way of simulating a change in air temperature, since it will vary hourly, daily and seasonally. A 10 °C step lasting for thousands of hours is therefore not realistic. Nevertheless, the simulation shows that changes in air temperature have a very slow impact on the temperature at burial depth.

To investigate more in detail how the temperature at burial depth is changing with a step change of 10 °C in air temperature, the temperature development at burial depth for the first 100 hours is depicted in figure 7.15.



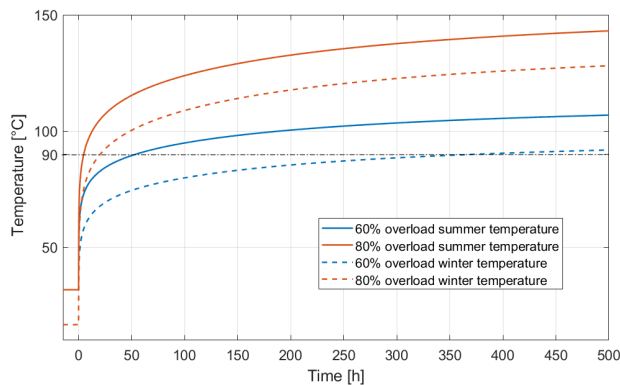
**Figure 7.15:** Temperature development at burial depth for a step increase in air ambient temperature for 100 hours.

Figure 7.15 shows that the temperature at burial depth increases by only 1 °C after applying a 10 °C air temperature step increase for 100 hours. For the first 15 hours or so, the temperature at cable burial depth remains constant.

The slow weather impact at burial depth that figure 7.14 and figure 7.15 show, justifies that changes in air ambient temperature during transients may be neglected in the dynamic rating calculations for buried cables. However, seasonal variations will impact the soil temperature at burial depth. Therefore, typical seasonal soil temperatures may be used for dynamic rating calculations for underground cables instead of taking real-time air ambient temperature into account.

## 7.5.2 Impact of seasonal variations of the soil

To show how seasonal temperature variations at burial depth of the cable will influence the calculated conductor temperature, the same overload conditions were applied to the cable with variations of the soil temperature. Winter temperature is assumed to be 0 °C, while summer temperature is set to 15 °C. Overload currents of 60% and 80% above rated is applied for 500 hours for both the winter and summer scenarios, as shown in figure 7.16. Prior to the overloading, an average load of 75% of rated current is assumed.



**Figure 7.16:** Impact of seasonal variations in summer and winter temperature at burial depth. Winter temperature is assumed to be 0 °C, while summer temperature is set to 15 °C.

Figure 7.16 shows that the cable may be overloaded for a longer period of time during winter temperatures. If the surrounding soil is assumed to be 15 °C at the start of the transient, the cable may be overloaded for 50 hours before the maximum conductor temperature of 90 °C is reached. However, by assuming soil temperature to be 0 °C, the same overload current may be applied for around 370 hours. This shows the importance of taking soil temperature at burial depth into account for dynamic rating of underground cables.



## Conclusions

In this thesis, several simulations are performed with an analytical thermal model developed according to the IEC standards for rating of power cables. The key findings of the thesis are:

- Transient temperature calculations from the analytical model compare well with the numerical modeling in COMSOL. In the case of a step load of rated current, the largest deviation in computed conductor temperature was only 2 °C. Moreover, the results show that the largest deviation occurs approximately 30 minutes after a change in applied current.
- Choosing appropriate values for soil properties has larger a impact on the accuracy of temperature calculations than the approximations made in the analytical model.
- The analytical algorithm only allows for one current step at a time. To obtain the total temperature rise due to a load profile consisting of multiple current steps, the temperature rise caused by each individual current step is added manually by the principle of superposition. This process could preferably be developed to a more automatic procedure.
- The results show that an interpretation of sheath temperature measurements can be useful for estimating conductor temperature. Such information may be obtained by measuring the time derivative of sheath temperature.
- It can be concluded that permitted overloading time periods will vary with applied overload current, conductor temperature limit and load history. In the case of an initial load of rated current and a 90 °C conductor temperature limit, an overload current of 60% can be applied for 30 hours. Due to large thermal time constants of the soil, permitted overloading time period will be increased manifold when the conductor temperature limit is extended to 100 °C and 110 °C.

- Based on the overloading case examples, the additional aging caused by increased temperatures was estimated. In the case of an overload current of 83% applied for 24 hours, the cable lifetime was reduced by approximately one month. This is only 0.2% of the total expected cable lifetime of 40 years.
- Moreover, it is shown that a 10 °C step change in air temperature lasting for 100 hours will only increase the soil temperature at burial depth with 1 °C. This slow impact of air temperature at burial depth justifies that variations in air temperature can be neglected during transient overloading. However, seasonal temperature variations at burial depth should be considered as it is shown that a buried cable can be overloaded for a longer period of time during winter conditions.



## Further work

Based on the research and obtained results in this thesis, the following proposals are suggested for further work:

- Perform measurements on a comparable laboratory setup to verify the transient temperature calculation method constructed in this thesis.
- Development of an application where a cable model and measurable data can be utilized by the utility to make decisions regarding for how long and to what extent the cable can operate at overload conditions.
- Further development of the established analytical model to allow for more complex load profiles.
- Because of the low heat transfer rate by natural convection in cable sections laying in air tunnels, this is often an ampacity limiting section of a buried cable system. The analytical model established in this thesis can be modified in order to calculate transient temperatures in these important cable sections.
- A cost/benefit analysis can be performed related to increased grid flexibility by allowing overloading for short time periods and the additional aging increased temperatures due to overloading will inflict on the cable insulation.

---

---

# Bibliography

- [1] BP. Energy Outlook, 2018. URL <https://www.bp.com/content/dam/bp/business-sites/en/global/corporate/pdfs/energy-economics/energy-outlook/bp-energy-outlook-2018.pdf>. Accessed: 2019-06-01.
- [2] Z. Liu. *Global Energy Interconnection 1st Edition*. Elsevier, 2015.
- [3] REN21. Renewables Global Futures Report, 2017. URL [http://www.ren21.net/wp-content/uploads/2017/10/GFR-Full-Report-2017\\_webversion\\_3.pdf](http://www.ren21.net/wp-content/uploads/2017/10/GFR-Full-Report-2017_webversion_3.pdf). Accessed: 2019-06-01.
- [4] C. J. Wallnerström, P. Hilber, P. Söderström, R. Saers, and O. Hansson. Potential of dynamic rating in Sweden. In *2014 International Conference on Probabilistic Methods Applied to Power Systems (PMAPS)*, pages 1–6, July 2014.
- [5] B. Leyland. Auckland central business district power failure. *Power Engineering Journal*, 12(3):109–114, June 1998.
- [6] J. Pilgrim, P. Lewin, A. Gorwadia, F. Waite, and D. Payne. Quantifying possible transmission network benefits from higher cable conductor temperatures. *IET Generation, Transmission Distribution*, 7(6):636–644, June 2013.
- [7] M. H. Shwehdi, M. A. Morsy, and A. Abugurain. Thermal aging tests on XLPE and PVC cable insulation materials of Saudi Arabia. In *2003 Annual Report Conference on Electrical Insulation and Dielectric Phenomena*, pages 176–180, October 2003.
- [8] M. Jensen. Overload Capacity of Polymer Insulated Medium Voltage Cables. Master’s thesis, Technical University of Denmark, Copenhagen, Denmark, 2011.
- [9] E. Ildstad. Compendium. TET4160 - Insulating Materials for High Voltage Applications, 2017.

- 
- [10] IEC 60287-1-1:2006. Electric cables - Calculation of the current rating - Part 1-1: Current rating equations (100% load factor) and calculation of losses - General. International standard, IEC, December 2006.
- [11] A. Safdarian, M. Z. Degefa, M. Fotuhi-Firuzabad, and M. Lehtonen. Benefits of Real-Time Monitoring to Distribution Systems: Dynamic Thermal Rating. *IEEE Transactions on Smart Grid*, 6(4):2023–2031, July 2015.
- [12] H. J. Li and K. C. Tan. Assessment of underground cable ratings based on distributed temperature sensing. *IEEE Transactions on Power Delivery*, 21(4):1763–1769, October 2006.
- [13] X. Feng and M. J. Mousavi. A framework for intelligent feeder overloading. In *2014 IEEE PES T&D Conference and Exposition*, pages 1–5, April 2014.
- [14] S. Talpur, C. J. Wallnerström, P. Hilber, and S. N. Saqib. Implementation of Dynamic Line Rating technique in a 130 kV regional network. In *17th IEEE International Multi Topic Conference 2014*, pages 477–482, December 2014.
- [15] G. J. Anders. *Rating of Electric Power Cables: Ampacity Computations for Transmission, Distribution and Industrial Applications*. McGraw Hill Professional, 1997.
- [16] D. A. Douglass and A. Edris. Real-time monitoring and dynamic thermal rating of power transmission circuits. *IEEE Transactions on Power Delivery*, 11(3):1407–1418, July 1996.
- [17] L. Chittock, J. Yang, D. Strickland, C. Harrap, and J. Mourik. Distribution network transformer thermal modelling parameter determination for dynamic rating applications. In *8th IET International Conference on Power Electronics, Machines and Drives (PEMD 2016)*, pages 1–6, April 2016.
- [18] J. Yang, L. Chittock, D. Strickland, and C. Harrap. Predicting practical benefits of dynamic asset ratings of 33KV distribution transformers. In *IET International Conference on Resilience of Transmission and Distribution Networks (RTDN) 2015*, pages 1–6, September 2015.
- [19] T. S. Jalal, N. Rashid, and B. van Vliet. Implementation of Dynamic Transformer Rating in a distribution network. In *2012 IEEE International Conference on Power System Technology (POWERCON)*, pages 1–5, October 2012.
- [20] B. Das, T. S. Jalal, and F. J. S. McFadden. Comparison and extension of IEC thermal models for dynamic rating of distribution transformers. In *2016 IEEE International Conference on Power System Technology (POWERCON)*, pages 1–8, September 2016.
- [21] E. Fernandez, I. Albizu, M. T. Bedialauneta, A. J. Mazon, and P. T. Leite. Review of dynamic line rating systems for wind power integration. *Renewable and Sustainable Energy Reviews*, 53:80 – 92, January 2016.

- 
- [22] Cigré Working Group B1.45. Thermal monitoring of cable circuits and grid operators' use of dynamic rating systems. In *B1 Insulated cables*, February 2019.
- [23] J. B. Prime and J. G. Valdes. System to Monitor the Conductor Temperature of Underground Cables. *IEEE Transactions on Power Apparatus and Systems*, PAS-100(1):143–153, January 1981.
- [24] S. P. Walldorf, A. Ernst, and S. Pancholi. A cost effective solution for increasing ratings on underground transmission cables-a case study. In *IEEE Transmission and Distribution Conference*, volume 1, pages 32–37, April 1999.
- [25] R. J. Nelson, T. F. Brennan, and J. S. Engelhardt. The application of real-time monitoring and rating to HPOF pipe cable systems. *IEEE Transactions on Power Delivery*, 4(2):850–856, April 1989.
- [26] G. Yilmaz and S. E. Karlik. A distributed optical fiber sensor for temperature detection in power cables. *Sensors and Actuators A: Physical*, 125(2):148 – 155, January 2006.
- [27] F. Ducheteauf. Optical fibers in power underground lines. In *Jicable 87 - Second International Conference on Polymer Insulated Power Cables*, pages 508–514, September 1987.
- [28] R. Stephens. Description of the state of the art methods to determine thermal rating of lines in real-time and their application in optimising power flow. *Session 2000 - Electrical Aspects of Overhead Lined*, 2000.
- [29] Cigré Working Group B2.36. Guide for Application of Direct Real-Time Monitoring Systems. In *B2 Overhead lines*, June 2012.
- [30] M. W. Davis. A new thermal rating approach: The real time thermal rating system for strategic overhead conductor transmission lines – Part I: General description and justification of the real time thermal rating system. *IEEE Transactions on Power Apparatus and Systems*, 96(3):803–809, May 1977.
- [31] D. A. Douglass. Weather-dependent versus static thermal line ratings (power overhead lines). *IEEE Transactions on Power Delivery*, 3(2):742–753, April 1988.
- [32] P. M. Callahan and D. A. Douglass. An experimental evaluation of a thermal line uprating by conductor temperature and weather monitoring. *IEEE Transactions on Power Delivery*, 3(4):1960–1967, October 1988.
- [33] J. S. Engelhardt and S. P. Basu. Design, installation, and field experience with an overhead transmission dynamic line rating system. In *Proceedings of 1996 Transmission and Distribution Conference and Exposition*, pages 366–370, September 1996.
- [34] C. J. Wallnerström, Y. Huang, and L. Söder. Impact From Dynamic Line Rating on Wind Power Integration. *IEEE Transactions on Smart Grid*, 6(1):343–350, January 2015.
-

- 
- [35] S. Talpur. Dynamic line rating implementation as an approach to handle wind power integration. Master's thesis, KTH Royal Institute of Technology, Stockholm, Sweden, 2013.
- [36] A. McLaughlin, M. Alshamali, J. Colandairaj, and S. Connor. Application of Dynamic Line Rating to Defer Transmission Network Reinforcement due to Wind Generation. In *2011 46th International Universities' Power Engineering Conference (UPEC)*, pages 1–6, September 2011.
- [37] J. Fu, D. J. Morrow, and S. Abdelkader. Integration of Wind Power into Existing Transmission Network by Dynamic Overhead Line Rating. In *Conference: 11th International Workshop on Large-Scale Integration of Wind Power into Power Systems as well as on Transmission Networks for Offshore Wind Power Plants*, November 2012.
- [38] J. Heckenbergerová and J. Hošek. Dynamic thermal rating of power transmission lines related to wind energy integration. In *2012 11th International Conference on Environment and Electrical Engineering*, pages 798–801, May 2012.
- [39] R. N. Patton, S. K. Kim, and R. Podmore. Monitoring and Rating of Underground Power Cables. *IEEE Transactions on Power Apparatus and Systems*, PAS-98(6): 2285–2293, November 1979.
- [40] S. Huang, W. Lee, and M. Kuo. An Online Dynamic Cable Rating System for an Industrial Power Plant in the Restructured Electric Market. *IEEE Transactions on Industry Applications*, 43(6):1449–1458, November 2007.
- [41] P. L. Lewin, J. E. Theed, A. E. Davies, and S. T. Larsen. Method for rating power cables buried in surface troughs. *IEE Proceedings - Generation, Transmission and Distribution*, 146(4):360–364, July 1999.
- [42] G. J. Anders, A. Napieralski, M. Zubert, and M. Orlikowski. Advanced modeling techniques for dynamic feeder rating systems. *IEEE Transactions on Industry Applications*, 39(3):619–626, May 2003.
- [43] M. Terracciano, S. Purushothaman, F. de León, and A. V. Farahani. Thermal Analysis of Cables in Unfilled Troughs: Investigation of the IEC Standard and a Methodical Approach for Cable Rating. *IEEE Transactions on Power Delivery*, 27(3):1423–1431, July 2012.
- [44] A. Sedaghat and F. de León. Thermal Analysis of Power Cables in Free Air: Evaluation and Improvement of the IEC Standard Ampacity Calculations. *IEEE Transactions on Power Delivery*, 29(5):2306–2314, October 2014.
- [45] J. A. Pilgrim, P. L. Lewin, S. T. Larsen, F. Waite, and D. Payne. Rating of Cables in Unfilled Surface Troughs. *IEEE Transactions on Power Delivery*, 27(2):993–1001, April 2012.

- 
- [46] P. L. Lewin, J. E. Theed, A. E. Davies, and S. T. Larsen. Method for rating power cables buried in surface troughs. *IEEE Proceedings - Generation, Transmission and Distribution*, 146(4):360–364, July 1999.
- [47] Y. Liang. Transient temperature analysis and short-term ampacity calculation of power cables in tunnel using SUPG finite element method. In *2013 IEEE Industry Applications Society Annual Meeting*, pages 1–4, October 2013.
- [48] J. A. Pilgrim, D. J. Swaffield, P. L. Lewin, S. T. Larsen, F. Waite, and D. Payne. Rating Independent Cable Circuits in Forced-Ventilated Cable Tunnels. *IEEE Transactions on Power Delivery*, 25(4):2046–2053, October 2010.
- [49] R. Olsen, G. J. Anders, J. Holboell, and U. S. Gudmundsdóttir. Modelling of Dynamic Transmission Cable Temperature Considering Soil-Specific Heat, Thermal Resistivity, and Precipitation. *IEEE Transactions on Power Delivery*, 28(3):1909–1917, July 2013.
- [50] R. Huang, J. A. Pilgrim, P. L. Lewin, and D. Payne. Dynamic cable ratings for smarter grids. In *IEEE PES ISGT Europe 2013*, pages 1–5, October 2013.
- [51] R. J. Millar. *A Comprehensive Approach to Real Time Power Cable Temperature Prediction and Rating in Thermally Unstable Environments*. PhD dissertation, Helsinki University of Technology, November 2006.
- [52] TWENTIES. Transmission system operation with a large penetration of wind and other renewable electricity sources in electricity networks using innovative tools and integrated energy solutions (TWENTIES), October 2013. URL <http://www.ewea.org/fileadmin/files/library/publications/reports/Twenties.pdf>. Accessed: 2019-02-10.
- [53] G. Balog, T. I. Nerby, and E. Kaldhuussæter. Cable temperature monitoring. In *Jicable 99 - Fifth International Conference on Insulated Power Cables*, volume 2, pages 577–581, June 1999.
- [54] Ø. Garvik and T. Lucignano. Distributed Temperature Sensing (DTS) on the NorNed HVDC Cable System. In *Cigré session*, 2018.
- [55] T. Lucignano. Personal email correspondence, 2019.
- [56] P. Leemans and M. Mampaey. Belgian experience with real time thermal rating system in combination with distributed temperature sensing techniques. In *Cigré session*, 2016.
- [57] IEC 60853-1:1985. Calculation of the cyclic and emergency current rating of cables. Part 1: Cyclic rating factor for cables up to and including 18/30(36) kV. International standard, IEC, January 1985.
- [58] G. J. Anders. *Rating of Electric Power Cables in Unfavorable Thermal Environment*. John Wiley & Sons, 2005.
-

- 
- [59] IEC 60853-2:1989. Calculation of the cyclic and emergency current rating of cables. Part 2: Cyclic rating of cables greater than 18/30 (36) kV and emergency ratings for cables of all voltages. International standard, IEC, September 1989.
- [60] IEC 60853-3:2002. Calculation of the cyclic and emergency current rating of cables. Part 3: Cyclic rating factor for cables of all voltages, with partial drying of the soil. International standard, IEC, February 2002.
- [61] O. T. Farouki. Thermal properties of soils. *CRREL Monograph 81-1*, page 3, December 1981.
- [62] E. Ildstad. *Underground power cable. Compendium in Course TET4195 - High Voltage Equipment*. NTNU, 2018.
- [63] S. Papadopoulos. Consideration of Ageing Factors in Extruded Insulation Cables and Accessories. *Electra No. 140*, 9(5):730–745, February 1992.
- [64] A. L. Dissado and J. C. Fothergill. *Electrical Degradation and Breakdown in Polymers*. The Redwood Press, 1992.
- [65] G. C. Montanari, G. Mazzanti, and L. Simoni. Progress in electrothermal life modeling of electrical insulation during the last decades. *IEEE Transactions on Dielectrics and Electrical Insulation*, 9(5):730–745, October 2002.
- [66] V. M. Montsinger. Loading Transformers By Temperature. *Transactions of the American Institute of Electrical Engineers*, 49:776 – 790, May 1930.
- [67] T. W. Dakin. Electrical insulation deterioration treated as a chemical rate phenomenon. *Transactions of the American Institute of Electrical Engineers*, 67(1):113–122, January 1948.
- [68] A. Harlin, M. Danikas, and P. Hyvönen. Polyolefin insulation degradation in electrical field below critical inception voltages. *Journal of Electrical Engineering*, 56, January 2005.
- [69] F. Aras, V. Alekperov, N. Can, and H. Kirkici. Aging of 154 kV underground power cable insulation under combined thermal and electrical stresses. *IEEE Electrical Insulation Magazine*, 23(5):25–33, September 2007.
- [70] G. Mazzanti and G. C. Montanari. A comparison between XLPE and EPR as insulating materials for HV cables. *IEEE Transactions on Power Delivery*, 12(1): 15–28, January 1997.
- [71] Y. J. Han, H. M. Lee, and Y. Shin. Thermal aging estimation with load cycle and thermal transients for XLPE-insulated underground cable. In *2017 IEEE Conference on Electrical Insulation and Dielectric Phenomenon (CEIDP)*, pages 205–208, October 2017.
- [72] Y. Liang and Y. M. Li. On-line dynamic cable rating for underground cables based on DTS and FEM. *WSEAS Transactions on Circuits and Systems*, 7:229–238, April 2008.



- 
- [73] M. Baù, N. Viafora, C. S. Hansen, L. M. B. Dall, T. Ebdrup, and F. F. da Silva. Steady state modelling of three-core wire armoured submarine cables: Power losses and ampacity estimation based on FEM and IEC. In *2016 51st International Universities Power Engineering Conference (UPEC)*, pages 1–6, September 2016.
- [74] J. J. Bremnes, L. Evenset, and R. Stølan. Power loss and inductance of steel armoured multi-core cables: comparison of IEC values with “2,5D” FEA results and measurements. In *Cigré Session*, August 2010.
- [75] R. Benato, S. D Sessa, M. Forzan, F. Gentilin, M. Marelli, and D. Pietribiasi. Finite Element model of a 3 m long three-core armoured submarine cable. In *2016 AEIT International Annual Conference (AEIT)*, pages 1–6, October 2016.
- [76] S. Sturm, K. L. Abken, and F. Berger. Estimating the losses in three-core submarine power cables using 2D and 3D FEA simulations. In *Jicable 2015 - 9th International Conference on Insulated Power Cables*, June 2015.
- [77] A. H. Steen. Transient Temperatures of Underground XLPE Power Cable. Master’s thesis, NTNU, Trondheim, Norway, June 2018.
- [78] COMSOL Multiphysics. Heat Transfer Module - User’s Guide, 2017.
- [79] G. C. Montanari and A. Motori. Thermal endurance evaluation of XLPE insulated cables. *Journal of Physics D: Applied Physics*, 24:1172–1181, July 1991.

---

---

# Appendix A

## Calculation of conductor and sheath temperature

This appendix shows how the transfer functions representing conductor and sheath temperature are derived from the thermal equivalent.

### Conductor temperature

The cable is represented by a two loop thermal network as in figure 5.3. For the first node ( $\theta_c$ ), which represents the conductor temperature, the transfer function may be written as.

$$H_c(s) = \frac{\theta_c}{W_c} = Z_{tot} \quad (\text{A.1})$$

In which  $Z_{tot}$  equals to:

$$Z_{tot} = \frac{1}{sQ_A + \frac{1}{T_A + \frac{1}{sQ_B + \frac{1}{T_B}}}} \quad (\text{A.2})$$

The steps involved to solve the complex fraction in equation A.2 are shown below:

$$H_c(s) = \frac{1}{sQ_A + \frac{1}{T_A + \frac{T_B}{sT_BQ_B + 1}}}$$

$$H_c(s) = \frac{1}{sQ_A + \frac{1 + sT_BQ_B}{T_A + T_B + sT_AT_BQ_B}}$$

$$H_c(s) = \frac{1}{\frac{1 + sT_BQ_B + sQ_A(T_A + T_B + sT_AT_BQ_B)}{T_A + T_B + sT_AT_BQ_B}}$$

---

Finally, the transfer function for the conductor node is:

$$H_c(s) = \frac{T_A + T_B + sT_A T_B Q_B}{1 + s(T_A Q_A + T_B Q_A + T_B Q_B) + s^2 T_A T_B Q_A Q_B} \quad (\text{A.3})$$

The coefficients  $T_{11}$  and  $T_{12}$  are calculated based on equation 3.10:

$$T_{11} = -\frac{x_{11}}{y_2} \frac{Z_{11} + a}{-a(-b + a)}$$

$$T_{11} = -\frac{T_A T_B Q_B}{T_A T_B Q_A Q_B} \frac{-\frac{T_A + T_B}{T_A T_B Q_B} + a}{-a(-b + a)}$$

$$T_{11} = -\frac{1}{Q_A} \frac{1}{a - b} \frac{T_A + T_B + a T_A T_B Q_B}{a T_A T_B Q_B}$$

$$T_{11} = \frac{1}{a - b} \left( \frac{1}{Q_A} - \frac{T_A + T_B}{a T_A T_B Q_A Q_B} \right)$$

but

$$ab = \frac{1}{T_A T_B Q_A Q_B}$$

Hence,  $T_{11}$  is given as:

$$T_{11} = \frac{1}{a - b} \left[ \frac{1}{Q_A} - b(T_A + T_B) \right] \quad (\text{A.4})$$

Doing the same for  $T_{12}$ :

$$T_{12} = \frac{1}{b - a} \left[ \frac{1}{Q_A} - a(T_A + T_B) \right] \quad (\text{A.5})$$

---

## Sheath temperature

In addition, the thermal network may be solved with respect to the sheath temperature,  $\theta_s$ , thus providing the sheath temperature as a function of time. The transfer function for the second node ( $\theta_s$ ) as in equation A.6.

$$H_s(s) = \frac{\theta_s}{W_c} = \frac{Z_b}{1 + sQ_A(T_A + Z_b)} \quad (\text{A.6})$$

In which  $Z_b$  is the total impedance "downstream" of the second node, given by:

$$Z_b = \frac{1}{sQ_B + \frac{1}{T_B}} \quad (\text{A.7})$$

The following steps shows the reduction of the complex fraction given in equation A.6:

$$H_s(s) = \frac{\frac{1}{sQ_B + \frac{1}{T_B}}}{1 + sQ_A \left( T_A + \frac{1}{sQ_B + \frac{1}{T_B}} \right)}$$

$$H_s(s) = \frac{\frac{T_B}{sT_BQ_B + 1}}{1 + sQ_A \left( T_A + \frac{T_B}{sT_BQ_B + 1} \right)}$$

$$H_s(s) = \frac{\frac{T_B}{sT_BQ_B + 1}}{1 + \frac{sQ_A(T_A + T_B + sT_AT_BQ_B)}{sT_BQ_B + 1}}$$

$$H_s(s) = \frac{\frac{T_B}{sT_BQ_B + 1}}{\frac{1 + s(T_AQ_A + T_BQ_A + T_BQ_B) + s^2T_AT_BQ_AQ_B}{sT_BQ_B + 1}}$$

Thus, the transfer function for the sheath node is given from equation A.8.

$$H_s(s) = \frac{T_B}{1 + s(T_AQ_A + T_BQ_A + T_BQ_B) + s^2T_AT_BQ_AQ_B} \quad (\text{A.8})$$

---

The coefficients  $T_{21}$  and  $T_{22}$  are calculated based on equation 3.10.

$$T_{21} = -\frac{x_2}{y_2} \frac{a}{-a(-b+a)}$$

$$T_{21} = -\frac{T_B}{T_A T_B Q_A Q_B} \frac{a}{-a(-b+a)}$$

$$T_{21} = \frac{1}{T_A Q_A Q_B (a-b)}$$

Since

$$ab = \frac{1}{T_A T_B Q_A Q_B}$$

Then  $T_{21}$  is:

$$T_{21} = \frac{T_B \cdot ab}{a-b} \tag{A.9}$$

When doing the same for  $T_{22}$ :

$$T_{22} = \frac{T_B \cdot a^2}{a-b^2} \tag{A.10}$$

---

# Appendix B

## Nomograms for exponential integral

The following rational approximations of the exponential integral is found in IEC 60853 [57] and used for calculations of influence of soil on transient temperature rise.

For  $0 \leq x \leq 1$ :

$$-Ei(-x) = -\ln(x) + \sum_{i=0}^5 a_i x^i$$

Where:

$$\begin{aligned} a_0 &= -0.5772 \\ a_1 &= 1.0000 \\ a_2 &= -0.2499 \\ a_3 &= 0.0552 \\ a_4 &= -0.0098 \\ a_5 &= 0.0011 \end{aligned}$$

For  $0 < x < 8$ :

$$-Ei(-x) = \frac{1}{xe^x} \left[ \frac{x^2 + a_1 x + a_2}{x^2 + b_1 x + b_2} \right]$$

Where:

$$\begin{aligned} a_1 &= 2.3347 \\ a_2 &= 0.2506 \\ b_1 &= 3.3307 \\ b_2 &= 1.6915 \end{aligned}$$

For values of  $x \geq 8$ ,  $-Ei(-x)$  is set to 0.

---

# Appendix C

## Overloading example

Figure C.1 shows the conductor temperature and time to reach maximum conductor temperature (90 °C for XLPE) for 60% (1120 A), 80% (1260 A) and 100% (1400 A). It was assumed that the average load prior to the overloading was 75% (525 A) of rated current. The figure also shows the corresponding measurable sheath temperatures for the various overload currents.

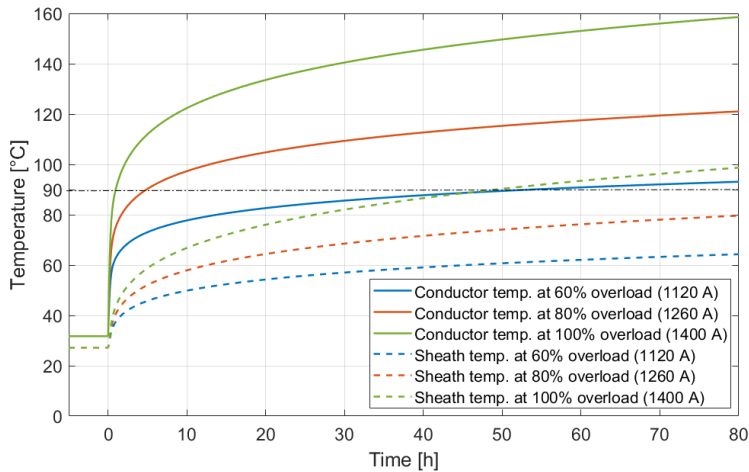


**Figure C.1:** Conductor temperature and time to reach maximum allowed conductor temperature for different overload scenarios. Average load prior to overloading was assumed to be 75% of rated current until steady-state conditions were obtained.

From the figure it can be seen that it takes around 50 hours to reach maximum allowed conductor temperature for the 60% overloading scenario. For the 80% overloading scenario it takes approximately five hours before the temperature limit is reached, whereas it takes about one hour for the 100% overloading scenario.



---

# Appendix D

## MATLAB source code

In the following appendix, the source code for transient temperature calculations with the analytical model is presented.

```
%Specification of cable dimensions, loading and ambient temperature
I0 = 700; %Loading
AmbTemp = 15; %Soil temperature at burial depth
A_cond = 300E-6; %Conductor area
D_cond = 20.5E-3; %Conductor diameter
D_ins = 30.10E-3; %Insulation diameter
t_ins = 4.8E-3; %Insulation thickness
t_sheath = 2.3E-3; %Sheath thickness
D_cable = 35.8E-3; %Cable diameter
L = 1; %Burial depth

%Specification of material properties
rho_ins = 1/0.286; %Thermal resistivity insulation (XLPE)
rho_sheath = 1/0.286; %Thermal resistivity sheath (PE)
rho_soil = 1; %Thermal resistivity soil
diff_soil = 5E-7; %Diffusivity of soil
c_ins = 2.4E6; %Specific heat insulation (XLPE)
c_sheath = 2.4E6; %Specific heat sheath (PE)
c_cond = 3.45E6; %Specific heat conductor (copper)
c_screen = 3.45E6; %Specific heat screen (copper)

%Calculation of thermal resistances, heat capacitances and Van Wormer
%coefficients from the thermal equivalent circuit in figure 5.2
T1 = rho_ins/(2*pi)*log(1+2*t_ins/D_cond);
%Thermal resistance of insulation layer
T3 = rho_sheath/(2*pi)*log(1+2*t_sheath/(D_cable - t_sheath));
%Thermal resistance of sheath layer
Qc = A_cond*c_cond;
%Heat capacitance of conductor
Qi = pi/4*(D_ins^2 - D_cond^2)*c_ins;
%Heat capacitance of insulation layer
Qj = pi/4*(D_cable^2 - (D_cable-2*t_sheath)^2)*c_sheath;
%Heat capacitance of sheath layer
Qs = pi/4*((D_cable-2*t_sheath)^2 - D_ins^2)*c_screen;
%Heat capacitance of screen layer
p = 1/(2*log(D_ins/D_cond))- 1/((D_ins/D_cond)^2-1);
%Van Wormer coefficient of the insulation layer
p_ = 1/(2*log(D_cable/(D_cable-2*t_sheath)))- 1/((D_cable/(D_cable-
2*t_sheath))^2-1); %Van Wormer coefficient of the sheath layer
```

---

```

%Calculation of thermal resistances, heat capacitances and other parameters
in the two-loop circuit in figure 5.3
TA = T1; %Thermal resistance TA
TB = T3; %Thermal resistance TB
QA = Qc + p*Qi; %Heat capacitance QA
QB = (1-p)*Qj + (Qs + p_*Qj); %Heat capacitance QA

%Coefficients to calculate T11 and T12 for the conductor temperature rise
%and T21 and T22 for the sheath temperature rise
M0 = 0.5*(TA*QA + TB*QB + TB*QA);
N0 = TA*QA*TB*QB;
a = (M0 + sqrt(M0^2 - N0))/N0;
b = (M0 - sqrt(M0^2 - N0))/N0;

T11 = 1/(a-b)*(1/QA - b*(TA + TB)); %Coefficient T11
T12 = TA + TB - T11; %Coefficient T12
T21 = 1/(a-b)*TB*a*b; %Coefficient T21
T22 = 1/(a-b^2)*TB*a^2; %Coefficient T22

%Setting the time duration and time step for simulation
time = 0:0.1:1000;

%Specifying properties to calculate initial heat loss in the conductor|
RefTemp = 20; %Reference temperature
S_cond = 5.8E7; %Electrical conductivity of
conductor (copper) copper at reference temperature
rho_cond = 1/S_cond; %Electrical resistivity of
conductor (copper) at reference temperature
R = rho_cond/A_cond; %Conductor (copper) resistance
alpha_cu = 0.0039; %Copper temperature coefficient
Wc = I0^2*R*(1+alpha_cu*(AmbTemp - RefTemp)); %Heat loss in conductor

%Transient temperature calculations of conductor and sheath temperature in
%a for loop
for t = time
    %Specifying x1 and x2 of the Exponential integral -Ei(-x)
    x1 = D_cable^2/(16*t*3600*diff_soil);
    x2 = L^2/(t*3600*diff_soil);
    %Specifying the limits of x1
    if (0 <= x1) && (x1 <= 1)
        %Coefficients in calculation of E1l for 0 <= x1 <= 1
        a0 = -0.5772;
        a1 = 1;
        a2 = -0.2499;
        a3 = 0.0552;
        a4 = 0.0098;
        a5 = 0.0011;
        %Calculation of E1l
        E1l = - log (x1) + a0*x1^0 + a1*x1^1 + a2*x1^2 + a3*x1^3 + a4*x1^4
            + a5*x1^5;
    elseif (1 < x1) && (x1 < 8)
        %Coefficients in calculation of E1l for 1 < x1 < 8
        a1 = 2.3347;
        a2 = 0.2506;
        b1 = 3.3307;
        b2 = 1.6815;

```

---

---

```

    %Calculation of Ei1
    Ei1 = 1/(x1*exp(x1))* ((x1^2 + a1*x1 + a2)/(x1^2 + b1*x1 + b2));
else
    Ei1 = 0;
end

%Specifying the limits of x2
if (0 <= x2) && (x2 <= 1)
    %Coefficients in calculation of Ei2 for 0 <= x2 <= 1
    a0 = -0.5772;
    a1 = 1;
    a2 = -0.2499;
    a3 = 0.0552;
    a4 = 0.0098;
    a5 = 0.0011;
    %Calculation of Ei2
    Ei2 = - log (x2) + a0*x2^0 + a1*x2^1 + a2*x2^2 + a3*x2^3 + a4*x2^4
    + a5*x2^5;
elseif (1 < x2) && (x2 < 8)
    %Coefficients in calculation of Ei2 for 1 < x2 < 8
    a1 = 2.3347;
    a2 = 0.2506;
    b1 = 3.3307;
    b2 = 1.6815;
    %Calculation of Ei2
    Ei2 = 1/(x2*exp(x2))* ((x2^2 + a1*x2 + a2)/(x2^2 + b1*x2 + b2));
else
    Ei2 = 0;
end

%Temperature rise due to influence of soil
TempSoilRise = Wc*rho_soil/(4*pi)*(Ei1-Ei2);
%Internal temperature rise of the conductor due to
%internal parts of the cable
CondTempCabRise = Wc*(T11*(1-exp(-a*t*3600))+T12*(1-exp(-b*t*3600)));
%Attainment factor for the conductor
Afac = CondTempCabRise / (Wc*(TA+TB));
%Total temperature rise of the conductor above ambient
CondTempTotRise = CondTempCabRise + TempSoilRise*Afac;
%Total conductor temperature
CondTempTot = CondTempTotRise + AmbTemp;

%Internal temperature rise of the sheath due to internal parts of the
%cable
ScreenTempCabRise = Wc*(T21*(1-exp(-a*t*3600))+T22*(1-exp(-
b*t*3600)));
%Attainment factor for the sheath
Afacs = ScreenTempCabRise / SteadyScreenTempCabRise;
%Total temperature rise of the sheath above ambient
ScreenTempTotRise = ScreenTempCabRise + TempSoilRise*Afacs;
%Total screen temperature
ScreenTempTot = ScreenTempTotRise + AmbTemp;

%Updating the conductor heat loss based on new conductor temperature
Wc = I0^2*R*(1+alpha_cu*(CondTempTot - RefTemp));
end

```

---

